



Published in final edited form as:

Cell Rep. 2022 April 05; 39(1): 110618. doi:10.1016/j.celrep.2022.110618.

## Affinity requirements for control of synaptic targeting and neuronal cell survival by heterophilic IgSF cell adhesion molecules

Shuwa Xu<sup>1,7,\*</sup>, Alina P. Sergeeva<sup>2</sup>, Phinikoula S. Katsamba<sup>3</sup>, Seetha Mannepilli<sup>3</sup>, Fabiana Bahna<sup>3</sup>, Jude Bimela<sup>3</sup>, S. Lawrence Zipursky<sup>4</sup>, Lawrence Shapiro<sup>3,5</sup>, Barry Honig<sup>2,3,5,6</sup>, Kai Zinn<sup>1,\*</sup>

<sup>1</sup>California Institute of Technology, Division of Biology and Biological Engineering, Pasadena, CA 91125, USA

<sup>2</sup>Department of Systems Biology, Columbia University Medical Center, New York, NY 10032, USA

<sup>3</sup>Zuckerman Mind Brain and Behavior Institute, Columbia University, New York, NY 10027, USA

<sup>4</sup>Department of Biological Chemistry, HHMI, David Geffen School of Medicine, University of California Los Angeles, Los Angeles, CA 90095, USA

<sup>5</sup>Department of Biochemistry and Molecular Biophysics, Columbia University, New York, NY 10032, USA

<sup>6</sup>Department of Medicine, Columbia University, New York, NY 10032, USA

<sup>7</sup>Lead contact

### SUMMARY

Neurons in the developing brain express many different cell adhesion molecules (CAMs) on their surfaces. CAM-binding affinities can vary by more than 200-fold, but the significance of these variations is unknown. Interactions between the immunoglobulin superfamily CAM DIP- $\alpha$  and its binding partners, Dpr10 and Dpr6, control synaptic targeting and survival of *Drosophila* optic lobe neurons. We design mutations that systematically change interaction affinity and analyze function *in vivo*. Reducing affinity causes loss-of-function phenotypes whose severity scales with the magnitude of the change. Synaptic targeting is more sensitive to affinity reduction than is cell survival. Increasing affinity rescues neurons that would normally be culled by apoptosis. By manipulating CAM expression together with affinity, we show that the key parameter controlling

This is an open access article under the CC BY-NC-ND license (<http://creativecommons.org/licenses/by-nc-nd/4.0/>).

\*Correspondence: shuwaxu@gmail.com (S.X.), zinnk@caltech.edu (K.Z.).

#### AUTHOR CONTRIBUTIONS

S.X., K.Z., and S.L.Z. conceived the project and wrote the majority of the paper. A.P.S., L.S., and B.H. wrote the section on mutant design and edited the remainder of the paper. S.X. and K.Z. designed the experiments. S.X. conducted the *in vivo* experiments and analyzed data. A.P.S., L.S., and B. H. designed the protein mutations and analyzed *in vitro* data. P.S.K. performed and analyzed surface plasmon resonance (SPR) experiments, and S.M., F.B., and J.B. produced and purified proteins.

#### DECLARATION OF INTERESTS

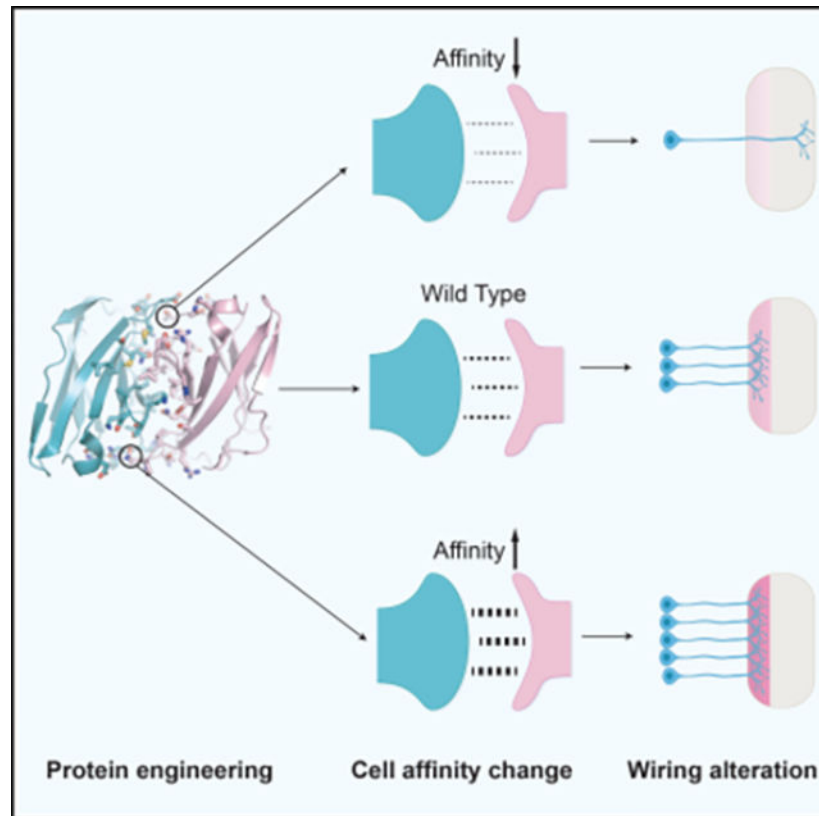
The authors declare no competing interests.

#### SUPPLEMENTAL INFORMATION

Supplemental information can be found online at <https://doi.org/10.1016/j.celrep.2022.110618>.

circuit assembly is surface avidity, which is the strength of adherence between cell surfaces. We conclude that CAM binding affinities and expression levels are finely tuned for function during development.

## Graphical Abstract



## In brief

Xu et al. demonstrate that altering the affinity of transsynaptic interactions between DIP- $\alpha$  and Dpr10 affects multiple aspects of circuit assembly in the *Drosophila* visual system.

## INTRODUCTION

Synapses in the central nervous systems of both vertebrates and invertebrates reside within dense and complex neuropils. During the development of “hard-wired” neural systems such as the *Drosophila* brain, axonal and dendritic processes choose genetically specified synaptic targets within environments where they have access to the surfaces of many non-target neurons. Roger Sperry’s chemoaffinity hypothesis proposed that individual neurons in such systems are labeled by molecules that give them unique identities. The modern version of this hypothesis is that cell adhesion molecule (CAM)-like cell-surface proteins (CSPs) expressed on interacting neuronal surfaces bind to each other and trigger downstream events that cause establishment of synaptic connections between appropriate partners.

CAM-like CSPs involved in synaptic targeting, which are denoted cell-recognition molecules (CRMs), include immunoglobulin superfamily (IgSF) proteins, cadherin superfamily proteins, leucine-rich repeat proteins, teneurins, and others. Each *Drosophila* neuron can express 100 or more different CAM genes during development (Barish et al., 2018; Konstantinides et al., 2018; Kurmangaliyev et al., 2019, 2020; Li et al., 2020; Özel et al., 2021; Tan et al., 2015). The number in vertebrates is comparable (Sarin et al., 2018). There are large variations in binding affinity even among CAMs in the same family (Honig and Shapiro, 2020). Loss or misexpression of CAMs can change synaptic connectivity, but the *in vivo* functions of CAM affinity variation have not been previously investigated.

The “Dpr-ome” interaction network was discovered in an *in vitro* “interactome” screen of IgSF CSPs (Özkan et al., 2013). Twenty-one Dpr proteins interact in a complex pattern with 11 DIPs (Carrillo et al., 2015; Cosmanescu et al., 2018; Tan et al., 2015). Most DIPs bind to multiple Dprs and vice versa. In the pupal optic lobe (OL), neurons expressing a particular DIP are often postsynaptic to neurons expressing a Dpr to which that DIP binds *in vitro* (Carrillo et al., 2015; Cosmanescu et al., 2018; Tan et al., 2015). Loss of DIPs and Dprs can alter synaptic connectivity and cause neuronal death, indicating that these proteins are CRMs (Ashley et al., 2019; Barish et al., 2018; Bornstein et al., 2021; Carrillo et al., 2015; Cheng et al., 2019; Courgeon and Desplan, 2019; Menon et al., 2019; Venkatasubramanian et al., 2019; Xu et al., 2018, 2019). The binding affinities of all interacting DIP/Dpr pairs have been measured using biophysical methods, and  $K_D$ s for homophilic and heterophilic binding vary by more than 100-fold, ranging from  $<2$  to  $>200$   $\mu\text{M}$  (Cosmanescu et al., 2018). The Dpr-ome provides an attractive system in which to examine if and how affinity variation contributes to the determination of synaptic-connectivity patterns.

DIP- $\alpha$  and Dpr10, the binding pair examined here, have one of the highest-affinity interactions in the network, with a  $K_D$  of 1.4  $\mu\text{M}$ . The high-resolution structures of DIP- $\alpha$  complexed with itself and with its Dpr partners have been determined, and binding *in vitro* has been characterized in detail using biophysical methods (Carrillo et al., 2015; Cosmanescu et al., 2018). DIP- $\alpha$  and Dpr10 are expressed in synaptically connected visual system neurons, and their interactions regulate synaptic targeting and cell survival for several neuronal types (Xu et al., 2018). Thus, the study of DIP- $\alpha$ ::Dpr10 interactions allows us to connect an analysis of *in vivo* function to *in vitro* measurements of binding affinity.

To understand how affinity affects CAM function *in vivo*, it is important to separate the effects of affinity alterations from those of the protein expression level. We introduced a series of designed mutations that either decrease or increase binding affinity into the *DIP- $\alpha$*  and *dpr10* loci, so that the mutant proteins would be expressed under the control of endogenous regulatory elements. We observed that reducing affinity causes loss-of-function (LOF) phenotypes, and that the severity of these phenotypes scales with the magnitude of affinity reduction. Synaptic targeting and cell survival have different affinity requirements.

Increasing affinity does not alter targeting, but it does affect cell survival. Our results suggest that DIP- $\alpha$ ::Dpr10 engagement controls a trophic-support pathway that counteracts cell-death pathways. When DIP- $\alpha$ ::Dpr10 interactions are sufficiently strengthened, the culling of visual system neurons by apoptosis that occurs during wild-type development

is eliminated. Changes in gene expression levels can compensate for alterations in protein binding affinity, indicating that avidity is the key parameter that determines the outcome of interactions between neurons mediated by these CAMs. The affinities and expression levels of DIP- $\alpha$  and its Dpr partners appear to be tuned so that the correct number of neurons survive and form appropriate synaptic connections.

## RESULTS

### Generation and selection of DIP- $\alpha$ and Dpr10 mutations that change DIP- $\alpha$ ::Dpr10 binding affinity

DIP- $\alpha$  binds to two Dprs, Dpr10 and Dpr6, with affinities of 1.4 and 2.0  $\mu\text{M}$ , respectively. DIP- $\alpha$  also binds to itself with an affinity of 24  $\mu\text{M}$  (Cheng et al., 2019; Cosmanescu et al., 2018; Sergeeva et al., 2020). We developed computational approaches that allowed the design of DIP- $\alpha$  and Dpr10 mutants that changed DIP- $\alpha$ ::Dpr10 binding affinity *in vitro* (Sergeeva et al., 2020). To determine how changes in affinity affect neuron-neuron recognition events, we selected a set of DIP- $\alpha$  and Dpr10 mutations for *in vivo* studies based on the following criteria: (1) the mutations should alter binding affinity between DIP- $\alpha$  and Dpr10 in a graded fashion so as to generate a set of proteins with affinities varying over a wide range, (2) the mutations should not change their specificity for binding to other DIP/Dpr proteins, and (3) the mutations should not have strong effects on the homophilic binding affinity of DIP- $\alpha$ .

Based on these criteria, we chose the designed DIP- $\alpha$  mutants K81Q ( $K_D = 31.8 \mu\text{M}$ , *DIP- $\alpha$ <sup>-20F</sup>*), the superscripts in mutant names indicate the direction and fold change in affinity relative to wild type), K81Q G74S ( $K_D = 68.0 \mu\text{M}$ , *DIP- $\alpha$ <sup>-50F</sup>*), and G74A ( $K_D = 0.9 \mu\text{M}$ , *DIP- $\alpha$ <sup>+2F</sup>*) and Dpr10 mutants V144K ( $K_D = 11.3 \mu\text{M}$ , *dpr10<sup>-8F</sup>*) and Q138D ( $K_D = 27.6 \mu\text{M}$ , *dpr10<sup>-20F</sup>*). To achieve a greater affinity range, we designed two additional Dpr10 mutants, V144K Q142E G99D ( $K_D = 50.0 \mu\text{M}$ , *dpr10<sup>-40F</sup>*) and Q142M ( $K_D = 0.19 \mu\text{M}$ , *Dpr10<sup>+10F</sup>*) (Figures 1B and 1C).  $K_D$  is further decreased to 0.10  $\mu\text{M}$  (a ~20-fold increase in affinity relative to wild type) when DIP- $\alpha$ <sup>+2F</sup> binds to *Dpr10<sup>+10F</sup>*. The locations of the designed mutations in the DIP- $\alpha$ ::Dpr10 interface are indicated in Figure 1A.

These Dpr10 and DIP- $\alpha$  mutations did not change the specificity of their binding to other DIP/Dpr proteins. Figure 1B shows binding isotherms for interactions of Dpr10 wild-type and mutant proteins with DIP- $\alpha$ , DIP- $\beta$ , and DIP- $\gamma$  (see Figure S1 for corresponding sensorgrams). DIP- $\beta$  is closest to DIP- $\alpha$  among all other DIPs in sequence and is also a Dpr10 binding protein, but with a much lower affinity ( $K_D = 33 \mu\text{M}$ ). DIP- $\gamma$  is not a Dpr10 binding protein ( $K_D > 1,000 \mu\text{M}$ ). Like wild-type Dpr10, all three mutant Dpr10 proteins interact more strongly with DIP- $\alpha$  than with DIP- $\beta$  and do not bind to DIP- $\gamma$  (Figure 1B). Figure 1C shows binding isotherms for DIP- $\alpha$  wild-type and mutant proteins to Dpr10, Dpr4, Dpr7, and Dpr12 (see Figure S1 for corresponding sensorgrams). Like wild-type DIP- $\alpha$ , none of the DIP- $\alpha$  mutants exhibits measurable binding to Dpr4, Dpr7, or Dpr12, which are members of non-cognate Dpr subgroups (Figure 1C).

Dpr10 is a monomer, while DIP- $\alpha$  can form dimers *in vitro* with a  $K_D$  of 24  $\mu\text{M}$  (Cosmanescu et al., 2018). The DIP- $\alpha$ /DIP- $\alpha$  and Dpr10/DIP- $\alpha$  interfaces are very

similar (root-mean-square deviation [RMSD] of 0.6 Å), and hence, changes in the surface used for heterophilic binding by DIP- $\alpha$  would be expected to also alter the homophilic DIP- $\alpha$ /DIP- $\alpha$  interface. To ensure that the DIP- $\alpha$  mutants retained the ability to homodimerize, we measured homophilic binding affinities of all DIP- $\alpha$  mutants using analytical ultracentrifugation (AUC). The homophilic binding  $K_D$ s for the three DIP- $\alpha$  mutant proteins are DIP- $\alpha$  G74A ( $DIP-\alpha^{+2F}$ ),  $K_D = 50 \mu\text{M}$ , DIP- $\alpha$  K81Q ( $DIP-\alpha^{-20F}$ )  $K_D = 19.6 \mu\text{M}$ , and DIP- $\alpha$  K81Q G74S ( $DIP-\alpha^{-50F}$ )  $K_D = 46 \mu\text{M}$  (Table S1). All mutants remain dimeric, and homophilic binding affinity is changed by no more than 2-fold. In summary, we have successfully created Dpr10 and DIP- $\alpha$  mutants with a wide affinity range that do not affect cognate binding preferences of DIPs and Dprs relative to non-cognate partners.

### DIP- $\alpha$ and Dpr10 affinity mutants are expressed normally *in vivo*

We introduced the chosen mutations into the endogenous *DIP- $\alpha$*  and *dpr10* genomic loci by a precise CRISPR-mediated knockin strategy (Zhang et al., 2014). We tested expression *in vivo* using antibodies specific for DIP- $\alpha$  and Dpr10 (Figures 2B and 2C). Wild-type DIP- $\alpha$  is expressed in three neuropil layers in the medulla region of the OL during mid-pupal development (48 h after puparium formation [APF]) (Xu et al., 2018) (Figure 2B'). All DIP- $\alpha$  affinity mutants were localized to the medulla neuropil and expressed in the same layers as wild type (Figures 2B''–2B'''). The DIP- $\alpha$ -expressing Dm1, Dm4, and Dm12 neurons project to the first (M1) and second (M3) DIP- $\alpha$  expressing layers (Figures 2A and 2B'). A large fraction of these neurons undergo cell death during pupal development in *DIP- $\alpha$*  null mutants (Xu et al., 2018). If our introduced mutations caused LOF phenotypes, they would be expected to cause a reduction in staining intensity in these two layers due to cell death even if they do not alter the levels of expression in individual cells. Another set of DIP- $\alpha$ -expressing neurons that project to a third layer (M10; yellow dotted line in Figure 2B') do not exhibit detectable cell death in null mutants, so we quantitated the expression levels of DIP- $\alpha$  mutant proteins in this layer. All three alleles showed similar expression levels to wild-type DIP- $\alpha$  in M10 (Figure 2D).

Dpr10 is expressed in two major medulla layers in the 48 h APF OL (Figure 2C'). All three Dpr10 affinity mutant proteins were expressed in the wild-type pattern (Figures 2C''–2C'''). Since no Dpr10-expressing OL neurons are known to exhibit cell death, we quantified Dpr10 expression levels in the whole neuropil. Two Dpr10 alleles were expressed at the same level as the wild type (Dpr10<sup>-8F</sup> and Dpr10<sup>-40F</sup>), while one was expressed at a slightly higher level than wild-type (Dpr10<sup>-20F</sup>) (Figure 2E).

### Reducing DIP- $\alpha$ ::Dpr10 affinity causes graded mistargeting of Dm12 neurons

Null *DIP- $\alpha$*  mutations or *dpr6 dpr10* double-null mutations disrupt targeting of Dm12 neurons and reduce survival of Dm1, Dm4, and Dm12 neurons (Xu et al., 2018). To determine how changing binding affinity between DIP- $\alpha$  and Dpr10 affects these processes, we first analyzed targeting of Dm12 neurons. Previously, we showed that *DIP- $\alpha$ <sup>null</sup>* Dm12 clones in a wild-type background target to a more proximal medulla layer, M8 (Figures 3B and 3G) (Xu et al., 2018). To better quantitate and visualize mistargeting in affinity mutants, we modified our methodologies by changing the genetic background and altering permeabilization, which allowed us to examine much larger numbers of neurons

using whole-animal mutants (see Method details and Immunohistochemistry). In *DIP-α<sup>null</sup>* mutants, about one-third of Dm12 neurons (~43 per OL) mistargeted to M8 (Figures 3B, 3G, and 3M). In *DIP-α<sup>-20F</sup>*, which has a ~20-fold reduction in DIP-α::Dpr10 binding affinity, ~5 (4%) of Dm12 neurons per OL mistargeted to M8 (Figures 3C and 3M). This number increased to ~20 (17%) in *DIP-α<sup>-50F</sup>*, which reduces affinity by ~50 fold (Figures 3D and 3M).

Dpr10 and Dpr6 are both expressed in the L3 lamina neuron, which forms synapses with Dm12 and Dm4 (Figure 2A). Loss of both Dprs (in a double-null mutant) causes the same mistargeting and cell-death phenotypes seen in *DIP-α* null mutants. *dpr10* or *dpr6* single mutants have much weaker phenotypes, indicating that the Dprs have partially redundant functions (Xu et al., 2018). Thus, to facilitate the analysis of the relationships between Dpr10 affinity and function, we knocked *dpr10* affinity mutations into the endogenous *dpr10* locus in a *dpr6* null mutant background. We analyzed Dm12 neurons in the three *dpr10* affinity mutants described above (*dpr10<sup>-8F</sup>*, *dpr10<sup>-20F</sup>*, and *dpr10<sup>-40F</sup>*). Animals expressing only wild-type Dpr10 but not Dpr6 (*dpr6<sup>null</sup>* single mutant), displayed a mild mistargeting phenotype in Dm12 neurons, with on average ~8 mistargeted Dm12 neurons per OL (Figures 3H and 3M). When Dpr10 affinity to DIP-α was reduced by 8-fold (in *dpr6<sup>null</sup> dpr1<sup>-8F</sup>*), ~14 mistargeted Dm12 neurons were observed (Figures 3I and 3M). A further reduction in affinity to 20-fold less than wild type (*dpr6<sup>null</sup> dpr10<sup>-20F</sup>*) caused a doubling of the number of mistargeted neurons, to ~29 cells (Figures 3J and 3M). Thus, in both *dpr10* and *DIP-α* mutants, the severity of Dm12 mistargeting scales with DIP-α::Dpr10 affinity reduction.

In these experiments, we observed that *dpr10* mutations that reduce affinity by 20- or 40-fold had stronger phenotypes than *DIP-α* mutations that reduce affinity by 20- or 50-fold (Figure 3M). However, as described above, *dpr10* affinity mutations were knocked into a *dpr6* null background, while *DIP-α* affinity mutant phenotypes were analyzed in a wild-type *dpr6* background. Because Dpr6 and Dpr10 are partially redundant (Xu et al., 2018), to accurately assess the relationships between phenotypic severity and DIP-α::Dpr10 binding affinity, we analyzed Dm12 neurons in *DIP-α* affinity mutants that also lacked Dpr6. The presence of the *dpr6<sup>null</sup>* mutations increased the extent of Dm12 mistargeting observed in *DIP-α* affinity mutants. For example, in the *DIP-α* mutant that decreases DIP-α::Dpr10 affinity by 20-fold, the number of mistargeted Dm12 neurons per OL increased from ~5 in *DIP-α<sup>-20F</sup>* to ~24 in *DIP-α<sup>-20F</sup> dpr6<sup>null</sup>* (Figures 3E and 3M). This number is similar to that observed in the *dpr10* affinity mutant that also reduces DIP-α::Dpr10 affinity by 20-fold (*dpr6<sup>null</sup> dpr10<sup>-20F</sup>*: ~29). In conclusion, in the absence of Dpr6, comparable phenotypic severity is observed for *DIP-α* or *dpr10* mutants that change DIP-α::Dpr10 affinity to a similar extent (Figure 3M).

### Different affinity thresholds control Dm12 targeting and cell survival

There are ~115 Dm12 neurons in a wild-type OL. In *DIP-α* or *dpr6 dpr10* null mutants, about 25 of these (~22%) die during development, reducing the total Dm12 complement to ~90 (Figure 3N) (Xu et al., 2018). Reducing DIP-α::Dpr10 binding affinity by 20-fold in a wild-type *dpr6* background did not cause any cell loss (*DIP-α<sup>-20F</sup>*). However, in the absence

of Dpr6 ( $DIP-\alpha^{-20F} dpr6^{null}$ ), ~9 Dm12 cells were lost. Removing Dpr6 from  $DIP-\alpha^{-50F}$  mutants produced a further increase in Dm12 cell loss, from ~9 to ~17 (Figure 3N).  $dpr10$  affinity mutants were examined in a  $dpr6$  null mutant background, and ~8 Dm12 cells were lost in  $dpr6$  single mutants. This number was not significantly changed by addition of  $dpr10^{-8F}$  or  $dpr10^{-20F}$  affinity mutations. However, in  $dpr6^{null} dpr10^{-40F}$  mutants, ~24 cells were lost (Figure 3N). Thus, in the absence of Dpr6, a 40- to 50-fold reduction in  $DIP-\alpha::Dpr10$  binding affinity produced a null or near-null cell-loss phenotype.

These results indicate that mistargeting and cell loss have different dependencies on  $DIP-\alpha::Dpr10$  binding affinity. We first observed a significant increase in mistargeting when affinity ( $K_D$ ) was reduced to 11.3  $\mu M$  in  $dpr6^{null} dpr10^{-8F}$ . When affinity was reduced by ~20-fold, in either  $dpr6^{null} dpr10^{-20F}$  ( $K_D = 27.8 \mu M$ ) or  $DIP-\alpha^{-20F} dpr6^{null}$  ( $K_D = 31.8 \mu M$ ), the penetrance of the mistargeting phenotype was about 50% of that observed in null mutants (Figures 3M and 3O). For cell loss, no increase above the  $dpr6$  null mutant penetrance was observed for  $DIP-\alpha^{-20F}$  or  $dpr6 dpr10^{-20F}$  mutants. A threshold of ~50% of the null penetrance was first exceeded in  $dpr6^{null} dpr10^{-40F}$  ( $K_D = 50.0 \mu M$ ) or  $DIP-\alpha^{-50F} dpr6^{null}$  ( $K_D = 68.0 \mu M$ ) (Figures 3N and 3O). Thus, we conclude that the 50% threshold for mistargeting is reached at a  $K_D$  of ~30  $\mu M$ , while the threshold for cell loss occurs at ~50  $\mu M$ . Note that there is more cell death in  $dpr6^{null} dpr10^{-40F}$  than in  $DIP-\alpha^{-50F} dpr6^{null}$  (Figure 3N). Perhaps in a  $dpr6^{null}$  background, the number of accessible  $DIP-\alpha$  molecules on Dm12 processes is in excess of the number of Dpr10 molecules on the axons of L3 and other presynaptic neurons in the M3 layer. This could account for cell-survival phenotypes being more sensitive to perturbation of Dpr10.

### A reduction in cell survival with decreasing affinity is also observed for Dm4 and Dm1 neurons

Dm4 and Dm1 processes do not mistarget in  $DIP-\alpha$  null or  $dpr6 dpr10$  double-null mutants (Figures 4A, 4D, and S2) (Xu et al., 2018). This suggests that  $DIP-\alpha::Dpr10$  interactions are redundant with other cues in directing the arbors of Dm4 and Dm1 neurons to the correct layers. However, survival of Dm4 and Dm1 neurons is affected by null  $DIP-\alpha$  or  $dpr6 dpr10$  mutations, so we were able to examine the effects of affinity mutations on cell survival for Dm4 and Dm1. We observed that Dm4 and Dm1 cell survival is also decreased in affinity mutants and that their survival is more sensitive to affinity reduction than that of Dm12 neurons. In  $DIP-\alpha^{-20F}/DIP-\alpha^{null}$  (null) mutants (wild type for  $dpr6$ ), cell loss was seen for Dm4 and Dm1 but not for Dm12 (Figures 3N, 4B, 4I, and S2). The stronger affinity mutant  $DIP-\alpha^{-50F}/DIP-\alpha^{null}$  exhibited as much cell loss as the null allele for Dm4 and Dm1 but had a weaker phenotype than the null for Dm12 (Figures 3N, 4C, 4I, and S2). Survival of Dm4 neurons was also more sensitive than survival of Dm12 neurons to affinity reduction by  $dpr10$  mutations. Dm4 cell loss is observed in  $dpr6^{null} dpr10^{-20F}$  mutants (Figures 4G and 4J), which have wild-type numbers of Dm12 neurons (Figure 3N). As for Dm12,  $dpr10$  affinity mutants have stronger phenotypes than the corresponding  $DIP-\alpha$  mutants, presumably because Dpr6 is still expressed in these  $DIP-\alpha$  mutant backgrounds. These data suggest that different cell types have different affinity thresholds for regulation of cell survival. This could be due to different levels of expression of  $DIP-\alpha$  in Dm4 and Dm1 neurons compared with Dm12 and/or to the use of alternative cell-death pathways.

### Increasing DIP- $\alpha$ ::Dpr10 affinity rescues Dm4 cell death

The analysis of affinity-reduction mutants described above shows that affinity thresholds exist for neuronal targeting and survival. When affinity is reduced to below these thresholds, neurons exhibit LOF phenotypes. We wished to also examine the consequences of increasing the affinity between DIP- $\alpha$  and Dpr10. Because DIP- $\alpha$ ::Dpr10 is already one of the highest-affinity interactions in the Dpr-ome, it is difficult to design mutants that increase affinity based on comparisons among DIP::Dpr binding interfaces. However, using position scanning mutagenesis via the FoldX computational algorithm (see STAR Methods), we were able to predict and experimentally validate two mutants that passed the selection criteria discussed above: DIP- $\alpha^{G74A}$  ( $K_D = 0.90 \mu\text{M}$ , DIP- $\alpha^{+2F}$ ) and Dpr10<sup>Q142M</sup> ( $K_D = 0.19 \mu\text{M}$ , Dpr10<sup>+10F</sup>). When DIP- $\alpha^{+2F}$  binds to Dpr10<sup>+10F</sup>,  $K_D$  is further decreased to  $0.10 \mu\text{M}$ , which represents a ~20-fold increase in affinity compared with wild type (Figures 5A and 5B).

Dm4, Dm12, and Dm1 exhibited normal layer targeting in both of the two increased affinity mutants (Figures 5C–5H and S3). We then analyzed cell-death phenotypes in Dm4 neurons. We have shown previously that Dm4 neurons are produced in excess in wild-type animals (~55 cells/OL) and that their number is reduced to ~40 cells/OL by apoptotic cell death during early pupal development (Figures 5I and 5J) (Xu et al., 2018). When apoptosis inhibitors (either baculovirus p35 protein or the *Drosophila* death-associated inhibitor of apoptosis 1 protein) are expressed in Dm4, the number of Dm4 neurons in adults remains at ~55 per OL (Figures 5I and 5J) (Xu et al., 2018). Loss of DIP- $\alpha$  or its Dpr partners causes increased Dm4 cell death, but it was unknown whether the natural Dm4 cell death that occurs in wild type is also regulated by DIP::Dpr interactions. To evaluate this, we counted adult Dm4 cell numbers in flies with increased affinity between DIP- $\alpha$  and Dpr10. In flies carrying two copies of *DIP- $\alpha^{+2F}$* , or one copy of *dpr10<sup>+10F</sup>* over wild-type *dpr10*, there was a small increase in Dm4 numbers, to ~45–48 cells/OL. Note that, because *dpr10<sup>+10F</sup>* was knocked into a *dpr6* null background, we analyzed *dpr10<sup>+10F</sup>* over a wild-type chromosome (*dpr6<sup>WT</sup>*, *dpr10<sup>WT</sup>*) to eliminate effects caused by loss of Dpr6, which in theory would counteract the effects of increasing affinity between DIP- $\alpha$  and Dpr10. In flies expressing both DIP- $\alpha^{+2F}$  and Dpr10<sup>+10F</sup> (*DIP- $\alpha^{+2F}$ /DIP- $\alpha^{WT}$* ; *dpr10<sup>+10F</sup>/dpr10<sup>WT</sup>*), there were ~55 Dm4 cells per OL, which is equal to the number observed when apoptosis inhibitors are expressed in wild type (Figures 5I and 5J). These results suggest that Dm4 cell death is entirely controlled by DIP- $\alpha$ 's interactions with its Dpr partners. Apoptosis in wild type is partially suppressed by a trophic-support pathway controlled by transsynaptic DIP::Dpr interactions. Decreasing trophic support by reducing DIP- $\alpha$ ::Dpr10 affinity leads to excess cell death, and increasing trophic support to above wild-type levels by increasing affinity suppresses normal cell death. The affinity and expression levels of DIP- $\alpha$  and its partners, and therefore the extent of apoptosis suppression, may have been adjusted by evolution to produce the desired number of adult Dm4 cells.

### An affinity threshold for induction of Dm4 mistargeting by ectopic Dpr10

Ectopic expression of Dpr10 in M10 is sufficient to induce mistargeting of the processes of DIP- $\alpha$ -expressing neurons (Xu et al., 2018). To analyze if this instructional role is also dependent on affinity, we made UAS lines for Dpr10 affinity mutants and tested their abilities to induce mistargeting. Both Dm4 and Dm12 neurons displayed misexpression-

induced mistargeting (Xu et al., 2018). Because of Dm4's smaller cell number (40 Dm4 s versus 115 Dm12 s) and thicker mistargeting axon branches, it is easier to quantitatively assess Dm4 mistargeting events. Thus, we used Dm4 neurons for analysis of mistargeting by Dpr10 affinity mutants.

T4 is not a synaptic partner of Dm4, but T4 processes come into contact with neurons that project to other medulla layers during early pupal development. They later segregate into the M10 layer of the medulla (Figure 2A). When endogenous Dpr10 is knocked out, and ectopic Dpr10 is misexpressed at high levels in T4 cells, it causes Dm4 neurons to send their processes to M10, bypassing their normal M3 target layer (Xu et al., 2018). We expressed Dpr10 affinity mutants in M10 using T4-Gal4. Dpr10 antibody staining revealed that M10 layer expression of UAS-Dpr10<sup>-8F</sup> and UAS-Dpr10<sup>-20F</sup> is comparable to that of wild-type UAS-Dpr10, while UAS-Dpr10<sup>-40F</sup> is expressed at 1.6-fold higher levels than wild type (Figure S4).

We analyzed each affinity mutant protein's ability to induce mistargeting of Dm4 neurons in a *dpr6 dpr10* double-null mutant background (Figure 6A–A'' and 6B–B''). About half of the Dm4 neurons undergo cell death due to the lack of Dpr6 and Dpr10, and as a result, there are fewer Dm4 processes in M3. The remaining ~20 Dm4 cells all target to the correct layer, so there must be other cues that direct Dm4 processes to M3 in the absence of DIP- $\alpha$  and its Dpr partners (Figures 4A–4H) (Xu et al., 2018). When wild-type Dpr10 was expressed in M10, Dm4 cell death was partially rescued (see below), and most of the Dm4 terminals were in the M10 layer, leaving few terminals in M3 (Figures 6C–C''). We counted Dm4 processes leaving M3 and targeting to M10 (Figures 6C–6F, yellow arrows) and divided that number by the total number of Dm4 cell bodies in the same sample, which we defined as the percentage of mistargeted Dm4 neurons. It sometimes exceeded 100%, indicating that some Dm4 neurons send out more than one process to the M10 layer (Figure 6G). Expressing Dpr10<sup>-8F</sup> in M10 caused about half as much Dm4 mistargeting as wild-type Dpr10, while expressing Dpr10<sup>-20F</sup> or Dpr10<sup>-40F</sup> produced almost no mistargeting (Figures 6D–6H).

We also tested the three Dpr10 affinity variants' abilities to induce Dm4 mistargeting in a wild-type animal, in which endogenous Dpr6 and Dpr10 in M3 compete with exogenous Dpr10 in M10. The percentage of mistargeted Dm4 neurons was reduced in this genetic background, but the three variants' relative ability to induce mistargeting remained the same (Figure 6G). The gain-of-function (GOF) mistargeting phenotype has more stringent affinity requirements than the LOF Dm12 targeting phenotype because Dpr10<sup>-8F</sup> ( $K_D = 11.3 \mu\text{M}$ ) induces mistargeting about half as well as wild-type Dpr10, while Dpr10<sup>-20F</sup> ( $K_D = 27.8 \mu\text{M}$ ) produces no mistargeting. This places the 50% penetrance threshold for this phenotype around 11  $\mu\text{M}$ , while for the LOF phenotype it is at ~30  $\mu\text{M}$  (Figure 3O).

### Cell-surface avidity is a key parameter controlling circuit assembly

The targeting and trophic-support functions of DIP- $\alpha$ ::Dpr10 interactions are both mediated through contact between neuronal cell surfaces. The contacting regions can be considered apposed two-dimensional sheets, each of which contains many DIP or Dpr molecules. The overall affinity of the cell surfaces for each other, known as avidity, is a combination of individual protein-protein binding affinity and protein density. It is likely that avidity

determines whether or not the strength of interaction between the two cells is sufficient to produce correct targeting and/or to suppress cell death. To examine this issue, we manipulated the expression levels of DIP and Dpr affinity mutants and examined the resulting phenotypes.

In the first set of experiments, we analyzed cell-number control in Dm4 neurons, comparing flies carrying one versus two copies of an affinity mutant *DIP-α* gene. Although ~6 Dm4 cells were rescued from cell death in *DIP-α<sup>+2F</sup>/DIP-α<sup>+2F</sup>* flies (Figure 5I), there was no change in the Dm4 cell number in *DIP-α<sup>+2F</sup>/DIP-α* animals (Figure 7A). In mutants that reduce affinity (*DIP-α<sup>-20F</sup>* and *DIP<sup>-50F</sup>*), there were significant differences in the Dm4 number between animals with two copies of a mutant gene versus those with one mutant copy over a null (Figure 7A). Thus, the Dm4 cell number is affected by *DIP-α* gene expression level, implying that avidity determines trophic-support levels. Removing a copy of wild-type *DIP-α* did not alter the Dm4 cell number (Figure 7A), suggesting that the phenotype is buffered around the wild-type condition. This may be a general phenomenon that explains why haploinsufficiency is rare in *Drosophila* and why most LOF mutations are recessive.

To examine whether expression levels affect neuronal targeting as well, we analyzed Dm12 mistargeting phenotypes in animals bearing one or two copies of wild-type or affinity mutant *dpr10* genes. Removing one copy of wild-type *dpr6* and one copy of wild-type *dpr10* produced no phenotypes (Figure S5A). In *dpr6<sup>null</sup>/dpr6<sup>null</sup>* (null) animals (bearing two copies of wild-type *dpr10*), there are on average ~8 Dm12 neurons that mistarget to M8. Loss of one copy of wild-type *dpr10* in the *dpr6* null mutant background produced a significant increase in mistargeting, with ~20 Dm12 cells mistargeting to M8 (Figure S5A). In *dpr10<sup>null</sup>/dpr10<sup>null</sup>* (null) animals (bearing two copies of wild-type *dpr6*), ~31 Dm12 neurons mistarget to M8, so mistargeting is more sensitive to the loss of Dpr10 than to the loss of Dpr6. Loss of one copy of wild-type *dpr6* in the *dpr10* null mutant background did not further increase mistargeting (Figure S5A). For affinity mutants, *dpr6* null mutant animals with one copy of *dpr10<sup>-8F</sup>* had stronger phenotypes than those with two copies (22 versus 14 mistargeted axons, respectively) (Figure S5A). However, there were no copy-number effects for *dpr10<sup>-20F</sup>* or *dpr10<sup>-40F</sup>*. In Figure 3M, we showed that there is a large (~2-fold) change in phenotypic penetrance between *dpr10<sup>-8F</sup>/dpr10<sup>-8F</sup>* and *dpr10<sup>-20F</sup>/dpr10<sup>-20F</sup>*, so mistargeting is likely sensitive to avidity alteration within that affinity range. However, Dpr10<sup>-20F</sup> is at the 50% penetrance affinity threshold, and Dpr10<sup>-40F</sup> is below that threshold, so copy-number changes for these alleles may have little effect. In conclusion, for both Dm4 cell-number control and Dm12 targeting, 2-fold changes in gene copy number can have strong effects on the phenotype in certain mutants, suggesting that the avidity of the interactions between the L3 and Dm4/Dm12 cell surfaces determines the functional consequences of these interactions.

### Overexpression of Dpr10 mutants can compensate for reduced protein binding affinity

The results described above indicate that *dpr10* LOF phenotypes are affected both by altering binding affinity and by changing avidity through alteration of gene expression levels through copy-number changes. To further examine this issue, we asked whether

overexpressing Dpr10 affinity mutants could compensate for a reduction in individual protein-protein binding affinity. *dpr10<sup>-20F</sup>* and *dpr10<sup>-40F</sup>* mutants both showed significant Dm4 cell loss. We overexpressed these mutant Dpr10 proteins in Dm4's synaptic partner, the L3 neuron, and analyzed rescue of Dm4 cell loss. We had previously shown that overexpressing wild-type Dpr10 in L3 fully rescues Dm4 cell loss in *dpr6<sup>null</sup> dpr10<sup>null</sup>* mutants (Xu et al., 2018). When we overexpressed Dpr10<sup>-20F</sup> or Dpr10<sup>-40F</sup> in L3, they fully rescued Dm4 cell loss in *dpr6<sup>null</sup> dpr10<sup>-20F</sup>* or *dpr6<sup>null</sup> dpr10<sup>-40F</sup>*, respectively, and were also able to rescue the *dpr6<sup>null</sup> dpr10<sup>null</sup>* phenotype (Figures 7B and S5B). These results show that increasing protein amounts can indeed compensate for reductions in individual protein-protein binding affinity (Figure 7C). Interestingly, they also indicate that our affinity mutants would have been classified as fully functional using conventional Gal4 rescue.

Finally, to test whether these results are specific to the Dm4 synaptic partner L3, we overexpressed different UAS-Dpr10 variants in T4 neurons, which project to M10. When wild-type Dpr10 was expressed in T4 cells, it was able to rescue cell loss due to the *dpr6 dpr10* double mutation but not fully to the wild-type number (34 versus 40) (Xu et al., 2018). Dpr10<sup>-20F</sup> or Dpr10<sup>-40F</sup> were able to rescue the Dm4 cell number to similar extents as wild-type Dpr10 (Figure S5C). The fact that rescue of Dm4 neuronal survival by T4-Gal4 is not complete even for wild-type Dpr10 could be due to the fact that the T4-Dm4 interaction is transient. Alternatively, there may be other proteins on the L3 surface that contribute to cell survival that are missing from T4 neurons. Note also that induction of Dm4 mistargeting by expression of Dpr10 in T4 cells has stringent affinity requirements (Dpr10<sup>-20F</sup> cannot induce mistargeting) (Figure 6H), while T4>Dpr10<sup>-20F</sup> works as well as wild type to rescue Dm4 cell death. This is likely because, in order to induce mistargeting, T4>Dpr10 must override the other cues that cause Dm4 to arborize in M3. By contrast, to rescue cell death, it is only necessary to supply enough Dpr10 signaling to replace that provided by the normal interaction between L3 and Dm4, and this can be done by increasing the expression levels of low-affinity mutants.

## DISCUSSION

In this paper, we systematically explore the impact of CAM affinity and avidity on synaptic connectivity in the *Drosophila* brain, focusing on the Dm4 and Dm12 medulla neurons, which are postsynaptic to the L3 lamina neuron in medulla layer M3. Dm4 and Dm12 express DIP- $\alpha$ , and L3 expresses its binding partners Dpr10 and Dpr6. The loss of interactions between DIP- $\alpha$  and its Dpr partners causes death of Dm4 and Dm12 neurons and mistargeting of Dm12 processes from layers M3 to M8 (Xu et al., 2018). To examine how alterations in DIP- $\alpha$ ::Dpr10 binding affinity affect targeting and cell survival, we introduced designed affinity mutations into the endogenous *DIP- $\alpha$*  and *dpr10* loci in the background of a *dpr6* null mutation so that the mutant proteins would be expressed at endogenous levels. We made fly lines expressing DIP- $\alpha$  mutants that bound to Dpr10 with ~20- and ~50-fold decreases in affinity relative to wild type, as well as a mutant with a ~2-fold increase in affinity. Dpr10 lines expressed mutants that bound to DIP- $\alpha$  with ~8-, ~20-, and ~40-fold decreases and a ~10-fold increase in affinity (Figures 1 and 2).

### Affinity requirements for synaptic targeting and survival are different

Targeting of Dm12 processes to M3, the medulla layer in which these neurons form synapses, is perturbed by mutations that reduce DIP- $\alpha$ ::Dpr10 binding affinity. In LOF mutants, Dm12 processes mistarget to M8 (Figure 3). Since Dpr6 and Dpr10 have partially redundant functions (Xu et al., 2018), to obtain an accurate estimate of the affinity threshold for targeting, we needed to examine both *dpr10* and *DIP- $\alpha$*  mutants in a *dpr6* null background. When we did this, we observed that a severity of ~50% of the null penetrance is observed when DIP- $\alpha$ ::Dpr10 affinity is reduced from 1.4 (wild-type) to ~30  $\mu$ M (Figure 3M).

Ectopic expression of Dpr10 in T4 neurons causes Dm12 and Dm4 processes to mistarget to M10 (Xu et al., 2018). We examined affinity requirements for this GOF phenotype using Dm4 because mistargeting is easier to quantitate for this neuron. Dm4 mistargeting through ectopic expression has more stringent affinity requirements than the LOF Dm12 mistargeting phenotype because Dpr10<sup>-8F</sup> ( $K_D = 11.3 \mu$ M) is only ~50% as effective as wild-type Dpr10, and Dpr10<sup>-20F</sup> ( $K_D = 27.8 \mu$ M) does not cause mistargeting (Figure 6H). This may be because there are other cues that direct Dm4 processes to M3 in the absence of DIP- $\alpha$  and Dpr10 (null mutations cause no Dm4 mistargeting), and ectopic Dpr10 expressed in M10 must overcome these cues in order to induce mistargeting.

To evaluate Dm12 cell survival, we counted Dm12 neurons in the same LOF genotypes used for examination of targeting. We found that survival has less stringent affinity requirements. The threshold of 50% of the null penetrance is only reached when affinity is reduced to 50  $\mu$ M (Figure 3N). Targeting and cell survival may use different downstream signaling components, accounting for the differential sensitivity of these phenotypes to affinity reduction. The signaling pathways downstream of DIP- $\alpha$  are likely to be mediated by unknown CSPs since DIP- $\alpha$  has no cytoplasmic domain (Özkan et al., 2013). Our preliminary analysis suggests that DIP- $\alpha$  is attached to the membrane by a glycosyl-phosphatidylinositol (GPI) linkage (data not shown).

### DIP- $\alpha$ ::Dpr10 affinity is finely tuned for control of Dm4 cell number

About 20% of the Dm4 cells that are originally generated are culled by apoptosis during early pupal development. There are ~40 Dm4 cells in a wild-type OL, but ~55 cells are present in adults if Dm4 apoptosis is blocked. In *DIP- $\alpha$*  null or *dpr6 dpr10* double-null mutants, ~50% of the remaining Dm4 neurons die, leaving ~20 cells in adults. This produces gaps in arbor coverage (Xu et al., 2018). Reducing affinity produces a gradual reduction in the Dm4 cell number, and the severity of cell loss scales with the magnitude of affinity reduction (Figure 4).

Increasing DIP- $\alpha$ ::Dpr10 affinity by ~20-fold rescues all of the cells that undergo apoptosis in wild type (Figure 5). We conclude that the affinity of DIP- $\alpha$ ::Dpr10 interactions is finely tuned to maintain an adult Dm4 cell assembly of ~40. When DIP- $\alpha$  on Dm4 binds to Dpr10, it activates a trophic-support pathway that counteracts apoptosis, and DIP- $\alpha$ ::Dpr10 interaction strength controls how much trophic support Dm4 neurons will receive. The balance between apoptosis and trophic support determines how many Dm4 neurons will

survive to adulthood. Since Dm4 neurons tile the medulla, the lateral extent of their arborizations within layer M3, and thus the sizes of their receptive fields, is inversely proportional to the number of Dm4 cells and, hence, dependent on the affinities of DIP- $\alpha$ ::Dpr6/10 interactions.

Extensive programmed cell death occurs in the OL during wild-type pupal development (Togane et al., 2012), and many OL neuron types are produced in excess. The affinities of binding between presynaptic and postsynaptic CRMs might control cell-number coordination in the developing visual system, ensuring that peripheral neurons in the retina and lamina are paired with the proper number of processing center neurons in the medulla. The use of protein binding affinity in such developmental process could provide neurons with the benefit of being able to use a single pair of interacting CRMs to both direct synaptic targeting and determine cell number.

### Relationships between avidity and affinity

We altered avidity while keeping individual protein-protein binding affinity fixed by changing the copy number of affinity mutant chromosomes and found that 2-fold copy-number changes can have strong effects on the extent of cell death and mistargeting. We also examined rescue by Gal4-driven overexpression of affinity mutants and found that an increase in protein level was able to fully compensate for the reduction of individual protein-protein interaction affinity (Figure 7 and S5). This illustrates the importance of introducing mutations into endogenous genes in order to assay subtle changes in protein function: increasing avidity through overexpression can allow even low-affinity mutants to behave like wild-type alleles, which will mask the functional changes in these mutant proteins.

### Affinity variation in CAM interactions and nervous-system assembly

Many previous studies have examined the effects of removing CAMs and altering CAM expression levels, and the results suggest that the summed affinity (avidity) of interactions between neuronal surfaces is important for the organization of nervous-system elements. For example, all lamina neurons express a single cadherin, CadN, and the concentric organization of the lamina cartridge is controlled by the relative levels of CadN. Neurons at the center of the cartridge express the highest levels of CadN, and R cells at the periphery express it at low levels. Manipulating CadN expression in different cells can change the relative positions of the neurons within the cartridge and alter its pattern of synapses (Schwabe et al., 2014). Similar mechanisms exist in the medulla (Trush et al., 2019).

The functions of binding affinities among individual CSPs have been examined in the immune system. For example, the affinities of interactions between T cell receptors and their peptide-major histocompatibility complex ligands control T cell specificities and activities (for review, see Stone et al., 2009). In the nervous system, however, the significance of CAM binding affinity has not been extensively studied. One paper examined affinity mutants of the SYG-1 and SYG-2 CAMs in *C. elegans*, which controls formation of synapses between motor neurons and muscles. Overexpressed SYG-1 mutant proteins with reduced affinity for SYG-2 are impaired in their ability to rescue the *syg-1* null mutant, suggesting that

SYG-1::SYG-2 binding affinity is important for function (Özkan et al., 2013). These results differ from our observations with DIP- $\alpha$ ::Dpr10, for which overexpression of low-affinity mutants fully rescued LOF phenotypes. The differences could be due to the strength of the drivers used for overexpressing proteins in *C. elegans* versus *Drosophila*.

Given the large number of CAMs expressed by a given neuron and the large variations in affinity among these CAMs (Kurmangaliyev et al., 2019, 2020; Li et al., 2020; Tan et al., 2015; Özel et al., 2021), it is likely that the affinities of individual CAM binding pairs have been selected by evolution. The Dpr-ome has seven specificity groups, each of which contains one to three DIPs that interact with one to five Dprs (Figure S1) (Carrillo et al., 2015; Cosmanescu et al., 2018; Sergeeva et al., 2020). The DIP::Dpr interactions that have been shown to be essential for brain wiring thus far (DIP- $\alpha$ ::Dpr10/6, DIP- $\gamma$ ::Dpr11, and DIP- $\delta$ ::Dpr12) and are of relatively high affinity (<10  $\mu$ M) (Bornstein et al., 2021; Carrillo et al., 2015; Courgeon and Desplan, 2019; Menon et al., 2019). By contrast, in the DIP-h/q/i and DIP- $\epsilon$ /z groups, all  $K_D$ s are >22  $\mu$ M (Figure S1C). This raises the question of whether low-affinity interactions might have different functions than those in the high-affinity groups.

Affinity alterations change the rates of association and/or dissociation of CAM complexes, and these rates might in turn affect the kinetics of transient associations between neuronal surfaces during development. Neurons form transient interactions with many other cells during axon/dendrite outgrowth and synaptogenesis. Some transient interactions, such as those with guidepost cells and intermediate targets, are genetically specified and help to determine the correct pattern of synaptic connections. Others probably occur randomly as a consequence of the dense packing of the developing neuropil. The ability of cells to form and break transient interactions may be facilitated by having a variety of CAMs with low affinity on their surfaces, each of which is present in many copies. This could allow cells to manipulate the strengths of their adhesive interactions with intermediate targets by modulating the levels of multiple CAMs that have partners on those targets. By contrast, if cells interacted with each other via a small number of copies of a few CAMs with much higher affinities, one or more CAMs might have to be completely removed in order to allow a neuron to break a transient interaction with an intermediate target. It will be interesting to determine whether the lower-affinity bindings might affect neuronal interactions with intermediate targets and if increasing affinity for these DIPs will cause defects in wiring.

### Limitation of the study

One limitation of this study is that we are unable to measure the levels of functional wild-type and affinity mutant DIP- $\alpha$  and Dpr10 proteins on neuronal cell surfaces. Whole-mount staining of the neuropil suggests that mutant proteins are expressed at comparable levels to wild type, but we cannot be sure that staining intensity accurately reports on cell-surface expression levels. Furthermore, although our study proves that changing the DIP- $\alpha$  or Dpr10 gene copy number or overexpressing the proteins affects phenotypes, we cannot determine exactly how these manipulations affect protein concentration on the cell surfaces.

DIP and Dpr proteins in general lack cytoplasmic domains or have very short cytoplasmic regions with no known functional domains or signaling motifs. We thus lack insights into the

mechanisms by which these proteins affect cellular signaling pathways that lead to changes in cell survival, axonal targeting, or synaptogenesis. This limits our understanding of how affinity alterations perturb these processes.

## STAR★METHODS

Detailed methods are provided in the online version of this paper and include the following:

### RESOURCE AVAILABILITY

**Lead contact**—Further information and requests for resources and reagents should be directed to and will be fulfilled by the lead contact, Dr. Shuwa Xu (shuwaxu@caltech.edu).

**Materials availability**—Plasmids generated in this study is available from the corresponding authors upon request.

Fly lines generated in this study is available from the corresponding authors upon request.

**Data and code availability**—This paper does not report original code. Data reported in this paper will be shared by the corresponding authors upon request. Any additional information required to reanalyze the data reported in this paper is available from the corresponding authors upon request.

### EXPERIMENTAL MODEL AND SUBJECT DETAILS

Flies were reared at 25°C on standard medium. For developmental analysis and sorting experiments white pre-pupae were collected and incubated for the indicated number of hours. Fly lines used in this study are listed in the Key Resources Table. Genotypes used for each experiment are provided in Table S2.

### METHOD DETAILS

**Generation of affinity mutant flies**—DIP- $\alpha^{+2F}$ , DIP- $\alpha^{-20F}$  and DIP- $\alpha^{-40F}$ : The genomic sequence of *DIP-a* including exon2-exon4 was first replaced with the sequence of attP-3XP3-DsRed-attP using a CRISPR-based knock-in strategy (Zhang et al., 2014), generating *DIP-a*-PRP flies. The same *DIP-a* genomic region was amplified from the wild-type fly genome using PCR and cloned into pBS-attB vector to make the donor plasmid. Mutations (G74A, K81Q, K81Q + G74S) that change DIP- $\alpha$  binding affinity to Dpr10 were introduced into the donor plasmid. Donor plasmids were injected into *DIP-a*-PRP flies generated above. Through FC31 recombinase-mediated cassette exchange, mutations were introduced into the fly genome (Injection completed at Bestgene. Inc). The detailed procedure was as in Zhang, et.al. 2014.

Dpr10<sup>-8F</sup>, Dpr10<sup>-20F</sup> Dpr10<sup>-40F</sup>: First, in Vas-Cas9(X); +/-; *dpr6*<sup>null</sup> flies, the genomic sequence of *dpr10* including 2 exons encoding the first Ig domain of dpr10 was replaced with the sequence of attP-3XP3-DsRed-attP using a CRISPR-based knock-in strategy (Zhang et al., 2014), generating *dpr6-*, *dpr10*-PRP flies. The same *dpr10* genomic region was amplified from the wild-type fly genome and cloned into pBS-attB vector to make the donor plasmid. Mutations (Q138D, Q142M, V144K, G99D + Q142E + V144K) that change Dpr10

binding affinity to DIP- $\alpha$  were introduced into the donor plasmid. Donor plasmids were injected into *dpr6<sup>-</sup>*, *dpr10-PRP* flies generated above. Through  $\Phi$ C31 recombinase-mediated cassette exchange, mutations were introduced into the fly genome (Injection completed at Bestgene. Inc). The detailed procedure was as in Zhang et al., (2014).

**Generation of UAS-transgenic flies**—cDNA encoding Dpr10-RD were cloned into the pJFRC28 vector (Pfeiffer et al., 2012) using standard cloning methods. The V5 sequence was inserted after signal peptide and before Ig1 for Dpr10 as described in Xu et al., (2018). Mutations that change Dpr10 affinity (Q138D, V144K, G99D + Q142E + V144K) were cloned into the above plasmids. Transgenes were inserted into the specific landing site at 28E7 by injection of fertilized embryos (Bestgene, Inc.). Plasmid and primer design were carried out using the software Snapgene. Plasmids and detailed sequences are available upon request.

**Immunohistochemistry**—Fly brains were dissected in PBS (137 mM NaCl, 2.7 mM KCl, 10 mM Na<sub>2</sub>HPO<sub>4</sub>, 1.8 mM KH<sub>2</sub>PO<sub>4</sub>) and fixed in PBS with 4% paraformaldehyde for 30 min at room temperature (RT). After 3 rinses with PBT at RT, samples were incubated in PBT (PBS 0.5% Triton-X100) containing 5% normal goat serum plus 5% normal donkey serum (blocking solution) for at least 1hr at RT. To visualize fine processes of mis-targeted Dm12 neurons, fly brains were fixed in 0.3% PBT plus 4% paraformaldehyde to increase tissue permeability. Brains were incubated at 4°C in primary and secondary antibodies for at least one day each with multiple PBT rinses at RT in between and afterwards. Brains were mounted in EverBrite mounting medium (Biotium).

The following primary antibodies were used in this study: chicken-anti-GFP (1:1000, Abcam ab13970); rabbit-anti-RFP (1:500, Clontech 600-401-379); mouse-anti-24B10 (Zipursky et al., 1984) (1:20, DSHB); mouse-anti-Brp (nc82) (1:10, DSHB); chicken-anti-V5 (1:500, Abcam 9113); mouse-anti-V5 (1:200, Life Technology, R96025); mouse-anti-DIP- $\alpha$  (4G11) (1:20) (Xu et al., 2018), mouse-anti-Dpr10 (1:5000) (Xu et al., 2018).

Secondary antibodies were used at 1:500 dilutions. From Jackson ImmunoResearch Lab: Alexa Fluor 488 donkey-anti-chicken (703-545-155); Alexa Fluor 488 donkey-anti-mouse (715-545-151); Alexa Fluor 594 donkey-anti-rabbit (711-585-152); From ThermoFisher Scientific: Alexa Fluor 647 goat-anti-mouse (A28181); Alexa Fluor 568 goat-anti-mouse (A-11004). From Life Technologies: Alexa Fluor 647 donkey-anti-mouse (A-21236).

**Microscopy and image analysis**—Confocal images were acquired on a Zeiss LSM880 confocal microscope. The staining patterns were reproducible between samples. However, some variation on the overall fluorescence signal and noise levels existed between sections and samples. Thus, proper adjustments of laser power, detector gain, and black level settings were made to obtain similar overall fluorescence signals.

Quantification of fluorescence intensity (in Figures 2, Figure 5): Samples were mounted dorsal up. For each sample, 15 slices of confocal images were taken starting from 50  $\mu$ m away from the surface, at 5  $\mu$ m step size. Each slice is analyzed separately against background signal for fluorescence intensity in ROI.

**Computational prediction of stabilizing mutations**—The crystal structure of Dpr10/DIP- $\alpha$  complex (PDBID: 6nrq) was used for FoldX calculations following a previously published protocol (Sergeeva et al., 2020) to evaluate the change in binding affinity upon mutations (G). Every interfacial residue of Dpr10 and DIP- $\alpha$  (33 positions on each side of the interface) was mutated into all possible amino acids amounting to 1254 G predictions. Of these, mutations corresponding to  $\Delta G < 0$  (stabilizing effect) were ranked and hits with largest stabilizing effect were probed experimentally.

**Surface plasmon resonance (SPR) binding experiments**—All DIP and Dpr proteins used in SPR experiments were expressed and purified as described previously (Sergeeva et al., 2020).

SPR binding assays were performed using a Biacore T100 biosensor equipped with a Series S CM4 sensor chip. To minimize artificial binding resulting from enhanced-avidity effects of oligomers binding to an immobilized ligand surfaces, DIPs are consistently used as ligands and immobilized over independent flow cells using amine-coupling chemistry in HBS pH 7.4 (10 mM HEPES, 150 mM NaCl) buffer at 25°C using a flow rate of 20  $\mu\text{L}/\text{min}$ . Dextran surfaces were activated for 7 min using equal volumes of 0.1M NHS (N-Hydroxysuccinimide) and 0.4M EDC(1-Ethyl-3-(3-dimethylaminopropyl) carbodiimide). Each protein of interest was immobilized at  $\sim 30 \mu\text{g}/\text{mL}$  in 10 mM sodium acetate, pH 5.5 until the desired immobilization level was achieved. The immobilized surface was blocked using a 4-min injection of 1.0 M ethanolamine, pH 8.5. Typical immobilization levels ranged between 760 and 980 RU. To minimize nonspecific binding the reference flow cell was blocked by immobilizing BSA in 10 mM sodium acetate, pH 4.25 for 3 min using a similar amine-coupling protocol as described above.

Binding analysis was performed at 25°C in a running buffer of 10 mM Tris-HCl, pH 7.2, 150 mM NaCl, 1 mM EDTA, 1 mg/mL BSA and 0.01% (v/v) Tween 20. Dpr analytes were prepared in running buffer and tested at nine concentrations using a three-fold dilution series ranging from 81 to 0.012  $\mu\text{M}$ . Similarly, Dpr10 was tested over the DIP- $\alpha$  and DIP- $\alpha$  G74A-immobilized surfaces at eight concentrations using a three-fold dilution series ranging from 27 to 0.012  $\mu\text{M}$ . Due to its high-affinity, Dpr10 Q142M was tested over DIP- $\alpha$  and DIP- $\alpha$  G74A-immobilized surfaces at nine concentrations using a three-fold dilution series ranging from 0.0014 to 9  $\mu\text{M}$ , but 0.012–81  $\mu\text{M}$  over both DIP- $\beta$  and DIP- $\gamma$ . Dpr10 Q138D was also tested at a concentration range of 27–0.012  $\mu\text{M}$  over all DIP surfaces, due to a limited protein expression of this mutant. In each experiment, every concentration was tested in duplicate. During a binding cycle, the association phase between each analyte and the immobilized molecule was monitored for either 30 or 40 s as indicated by the plotted sensorgrams, followed by 120-s dissociation phase, each at 50  $\mu\text{L}/\text{min}$ . At the end of the dissociation phase the signal returned to baseline thus eliminating the need for a regeneration step. The last step was buffer wash injection at 100  $\mu\text{L}/\text{min}$  for 60 s. The analyte was replaced by buffer every two or three binding cycles to double-reference the binding signals by removing systematic noise and instrument drift. The responses between 25 and 29 s, at which point the binding reactions achieve equilibrium as observed by the flat binding responses, were plotted against the concentration of analyte. The data was fit to 1:1 interaction model and the  $K_D$  was calculated as the analyte concentration that would yield

0.5  $R_{\max}$  (Rich and Myszka, 2009). The data was processed using Scrubber 2.0 (BioLogic Software).

## QUANTIFICATION AND STATISTICAL ANALYSIS

Images were analyzed with ImageJ software. Cell number counting were facilitated with Fiji (Schindelin et al., 2012) plugin “Clear-Volume” (Royer et al., 2015) and Imaris (Bitplane Inc) software (semi-automatically with hand-correction). Statistical analysis was done using Prism software. All data are shown as mean  $\pm$  standard deviation (SD). Statistical test used is indicated in each figure. p value is indicated in figure legend.

## Supplementary Material

Refer to Web version on PubMed Central for supplementary material.

## ACKNOWLEDGMENTS

We thank the Richard Mann Lab for general discussions. Confocal imaging was completed in the Caltech Biological Imaging Facility. This work was supported by NIH grants R37NS028182 and RO1NS096509 (K.Z.) and NSF grant MCB-1914542 (B.H.).

## REFERENCES

- Ashley J, Sorrentino V, Lobb-Rabe M, Nagarkar-Jaiswal S, Tan L, Xu S, Xiao Q, Zinn K, and Carrillo RA (2019). Transsynaptic interactions between IgSF proteins DIP- $\alpha$  and Dpr10 are required for motor neuron targeting specificity. *Elife* 8, e42690. [PubMed: 30714906]
- Barish S, Nuss S, Strunilin I, Bao S, Mukherjee S, Jones CD, and Volkan PC (2018). Combinations of DIPs and Dprs control organization of olfactory receptor neuron terminals in *Drosophila*. *PLoS Genet.* 14, e1007560. [PubMed: 30102700]
- Bornstein B, Meltzer H, Adler R, Alyagor I, Berkun V, Cummings G, Reh F, Keren-Shaul H, David E, Riemensperger T, et al. (2021). Transneuronal Dpr12/DIP-8 interactions facilitate compartmentalized dopaminergic innervation of *Drosophila* mushroom body axons. *EMBO J* 40, e105763. [PubMed: 33847376]
- Carrillo RA, Özkan E, Menon KP, Nagarkar-Jaiswal S, Lee P-T, Jeon M, Birnbaum ME, Bellen HJ, Garcia KC, and Zinn K (2015). Control of synaptic connectivity by a network of *Drosophila* IgSF cell surface proteins. *Cell* 163, 1770–1782. [PubMed: 26687361]
- Cheng S, Ashley J, Kurlito JD, Lobb-Rabe M, Park YJ, Carrillo RA, and Özkan E (2019). Molecular basis of synaptic specificity by immunoglobulin superfamily receptors in *Drosophila*. *Elife* 8, e41028. [PubMed: 30688651]
- Cosmanescu F, Katsamba PS, Sergeeva AP, Ahlsén G, Patel SD, Brewer JJ, Tan L, Xu S, Xiao Q, Nagarkar-Jaiswal S, et al. (2018). Neuron-subtype-specific expression, interaction affinities, and specificity determinants of DIP/dpr cell recognition proteins. *Neuron* 100, 1385–1400. [PubMed: 30467080]
- Courgeon M, and Desplan C (2019). Coordination between stochastic and deterministic specification in the *Drosophilavisual* system. *Science* 366, eaay6727–13. [PubMed: 31582524]
- Honig B, and Shapiro L (2020). Adhesion protein structure, molecular affinities, and principles of cell-cell recognition. *Cell* 181, 520–535. [PubMed: 32359436]
- Konstantinides N, Kapuralin K, Fadil C, Barboza L, Satija R, and Desplan C (2018). Phenotypic convergence: distinct transcription factors regulate common terminal features. *Cell* 174, 622–635.e13. [PubMed: 29909983]
- Kurmangaliyev YZ, Yoo J, Locascio SA, and Lawrence Zipursky S (2019). Modular transcriptional programs separately define axon and dendrite connectivity. *Elife* 8, e50822. [PubMed: 31687928]

- Kurmangaliyev YZ, Yoo J, Valdes-Aleman J, Sanfilippo P, and Zipursky SL (2020). Transcriptional programs of circuit assembly in the *Drosophila* visual system. *Neuron* 108, 1045–1057.e6. [PubMed: 33125872]
- Li J, Han S, Li H, Udeshi ND, Svinkina T, Mani DR, Xu C, Guajardo R, Xie Q, Li T, et al. (2020). Cell-surface proteomic profiling in the fly brain uncovers wiring regulators. *Cell* 180, 1–14. [PubMed: 31836194]
- Menon KP, Kulkarni V, Takemura S, Anaya M, and Zinn K (2019). Interactions between Dpr11 and DIP- $\gamma$  control selection of amacrine neurons in *Drosophila* color vision circuits. *Elife* 8, e48935. [PubMed: 31692445]
- Özel MN, Simon F, Jafari S, Holguera I, Chen YC, Benhra N, El-Danaf RN, Kapuralin K, Malin JA, Konstantinides N, et al. (2021). Neuronal diversity and convergence in a visual system developmental atlas. *Nature* 589, 88–95. [PubMed: 33149298]
- Özkan E, Carrillo RA, Eastman CL, Weiszmann R, Waghray D, Johnson KG, Zinn K, Celniker SE, and Garcia KC (2013). An extracellular interactome of immunoglobulin and LRR proteins reveals receptor-ligand networks. *Cell* 154, 228–239. [PubMed: 23827685]
- Pecot MY, Chen Y, Akin O, Chen Z, Tsui CYK, and Zipursky SL (2014). Sequential axon-derived signals couple target survival and layer specificity in the *Drosophila* visual system. *Neuron* 82, 320–333. [PubMed: 24742459]
- Pfeiffer BD, Truman JW, and Rubin GM (2012). Using translational enhancers to increase transgene expression in *Drosophila*. *Proc. Natl. Acad. Sci. U S A* 109, 6626–6631. [PubMed: 22493255]
- Rich R, and Myszka D (2009). Extracting affinity constants from biosensor binding responses. In *Label-Free Biosensors: Techniques and Applications*, Cooper M, ed. (Cambridge University Press), pp. 48–84.
- Royer LA, Weigert M, Günther U, Maghelli N, Jug F, Sbalzarini IF, and Myers EW (2015). ClearVolume: open-source live 3D visualization for lightsheet microscopy. *Nat. Methods* 12, 480–481. [PubMed: 26020498]
- Sarin S, Zuniga-Sanchez E, Kurmangaliyev YZ, Cousins H, Patel M, Hernandez J, Zhang KX, Samuel MA, Morey M, Sanes JR, et al. (2018). Role for Wnt signaling in retinal neuropil development: analysis via RNA-seq and in vivo somatic CRISPR mutagenesis. *Neuron* 98, 109–126.e8. [PubMed: 29576390]
- Schindelin J, Arganda-Carreras I, Frise E, Kaynig V, Longair M, Pietzsch T, Preibisch S, Rueden C, Saalfeld S, Schmid B, et al. (2012). Fiji: an open-source platform for biological-image analysis. *Nat. Methods* 9, 676–682. [PubMed: 22743772]
- Schwabe T, Borycz JA, Meinertzhagen IA, and Clandinin TR (2014). Differential adhesion determines the organization of synaptic fascicles in the *Drosophila* visual system. *Curr. Biol.* 24, 1304–1313. [PubMed: 24881879]
- Sergeeva AP, Katsamba PS, Cosmanescu F, Brewer JJ, Ahlsen G, Mannepalli S, Shapiro L, and Honig B (2020). DIP/Dpr interactions and the evolutionary design of specificity in protein families. *Nat. Commun.* 11, 1–14. [PubMed: 31911652]
- Stone JD, Chervin AS, Stone JD, Chervin AS, and Kranz DM (2009). T-cell receptor binding affinities and kinetics: Impact on T-cell activity and specificity. *Immunology* 126, 165–176. 10.1111/j.1365-2567.2008.03015.x. [PubMed: 19125887]
- Tan L, Zhang KX, Pecot MY, Nagarkar-Jaiswal S, Lee P-T, Takemura S, McEwen JM, Nern A, Xu S, Tadros W, et al. (2015). Ig superfamily ligand and receptor pairs expressed in synaptic partners in *Drosophila*. *Cell* 163, 1756–1769. [PubMed: 26687360]
- Togane Y, Ayukawa R, Hara Y, Akagawa H, Iwabuchi K, and Tsujimura H (2012). Spatio-temporal pattern of programmed cell death in the developing *Drosophila* optic lobe. *Dev. Growth Differ.* 54, 503–518. [PubMed: 22587328]
- Trush O, Liu C, Han X, Nakai Y, Takayama R, Murakawa H, Carrillo JA, Takechi H, Hakeda-Suzuki S, Suzuki T, et al. (2019). N-cadherin orchestrates self-organization of neurons within a columnar unit in the *Drosophila* medulla. *J. Neurosci.* 39, 5861–5880. [PubMed: 31175213]
- Venkatasubramanian L, Guo Z, Xu S, Tan L, Xiao Q, Nagarkar-Jaiswal S, and Mann RS (2019). Stereotyped terminal axon branching of leg motor neurons mediated by igsf proteins dip- $\alpha$  and dpr10. *Elife* 8, e42692. [PubMed: 30714901]

- Xu C, Theisen E, Maloney R, Peng J, Santiago I, Yapp C, Werkhoven Z, Rumbaut E, Shum B, Tarnogorska D, et al. (2019). Control of synaptic specificity by establishing a relative preference for synaptic partners. *Neuron* 103, 1–13. [PubMed: 31271753]
- Xu S, Xiao Q, Cosmanescu F, Sergeeva AP, Yoo J, Lin Y, Katsamba PS, Ahlsen G, Kaufman J, Linaval NT, et al. (2018). Interactions between the Ig-superfamily proteins DIP- $\alpha$  and Dpr6/10 regulate assembly of neural circuits. *Neuron* 100, 1369–1384.e6. [PubMed: 30467079]
- Zhang X, Koolhaas WH, and Schnorrer F (2014). A versatile two-step CRISPR- and RMCE-based strategy for efficient genome engineering in *Drosophila*. *G3 (Bethesda)*. 4, 2409–2418. [PubMed: 25324299]
- Zipursky SL, Venkatesh TR, Teplow DB, and Benzer S (1984). Neuronal development in the *Drosophila* retina: monoclonal antibodies as molecular probes. *Cell* 36, 15–26. [PubMed: 6420071]

**Highlights**

- DIP- $\alpha$ ::Dpr10 binding affinity is important for layer-specific circuit assembly
- Cell death and synaptic targeting have different affinity thresholds
- Increasing DIP- $\alpha$ ::Dpr10 binding affinity blocks neuronal culling through apoptosis
- Cell-surface avidity is determined by protein-expression levels and binding affinity

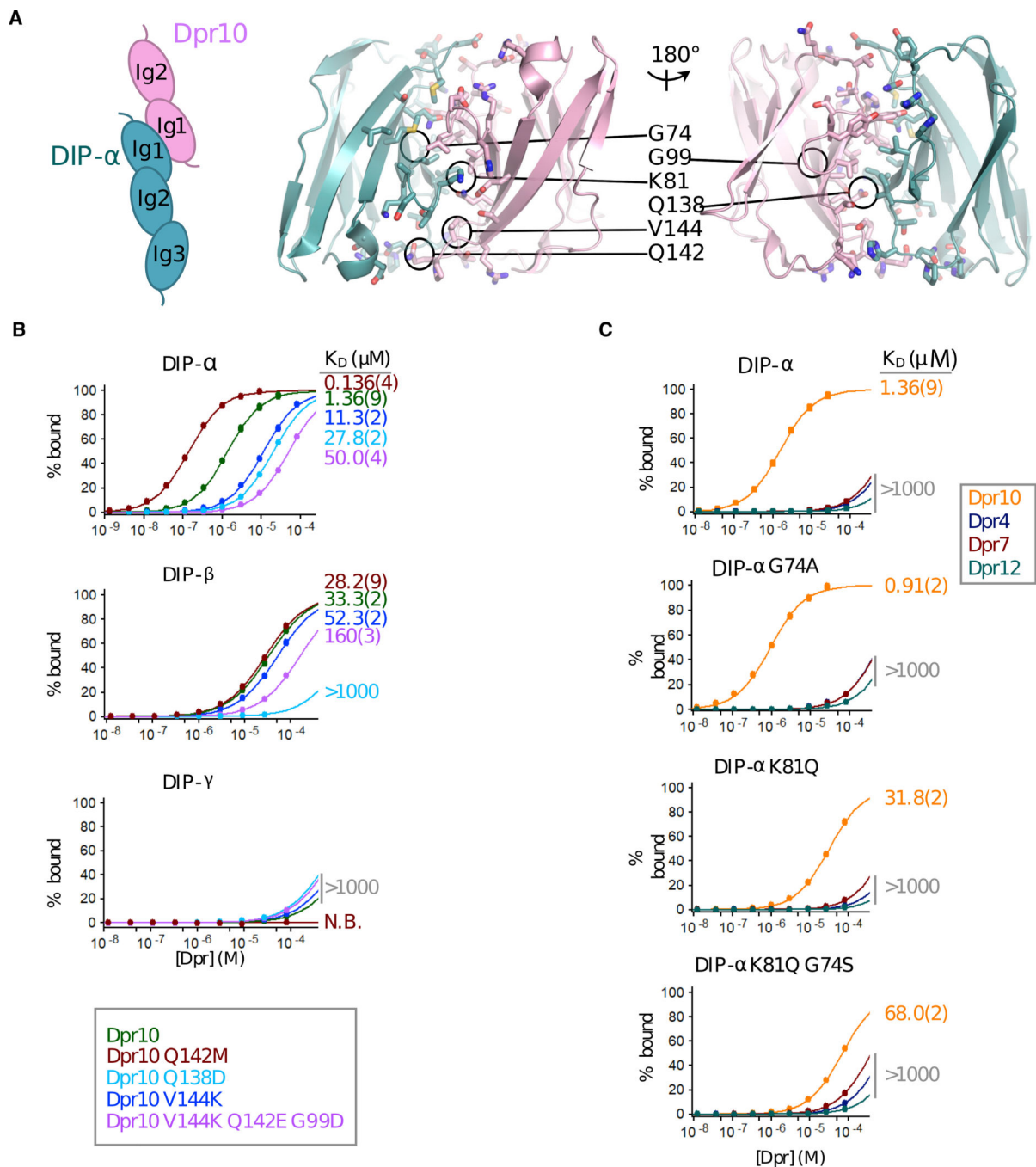


**Figure 1. Biophysical analysis of interactions of DIP-α and Dpr10 mutants**

(A) Schematic representation of DIP-α/Dpr10 heterodimer formed between N-terminal immunoglobulin 1 (Ig1) domains of DIP-α (in cyan) and Dpr10 (in pink), left, and the structure of the DIP-α/Dpr10 interface (PDB: 6NRQ), right. Interfacial residues (within 6Å of the opposing protomer) are depicted as sticks, and mutated positions are encircled and marked.

(B and C) Binding isotherms from SPR binding experiments.

(B) Dpr10 and its mutants binding to DIP-α, DIP-β, and DIP-γ.

(C) Dprs 10, 4, 7, and 12 binding to DIP- $\alpha$  and its mutants.

The binding isotherms and the  $K_{DS}$  are color coded according to the legend shown to the right of each panel.  $K_{DS} > 1,000 \mu\text{M}$  describing multiple interactions are shown in gray.

N.B., no binding detected. The binding responses corresponding to the SPR experiments are shown in Figure S1.

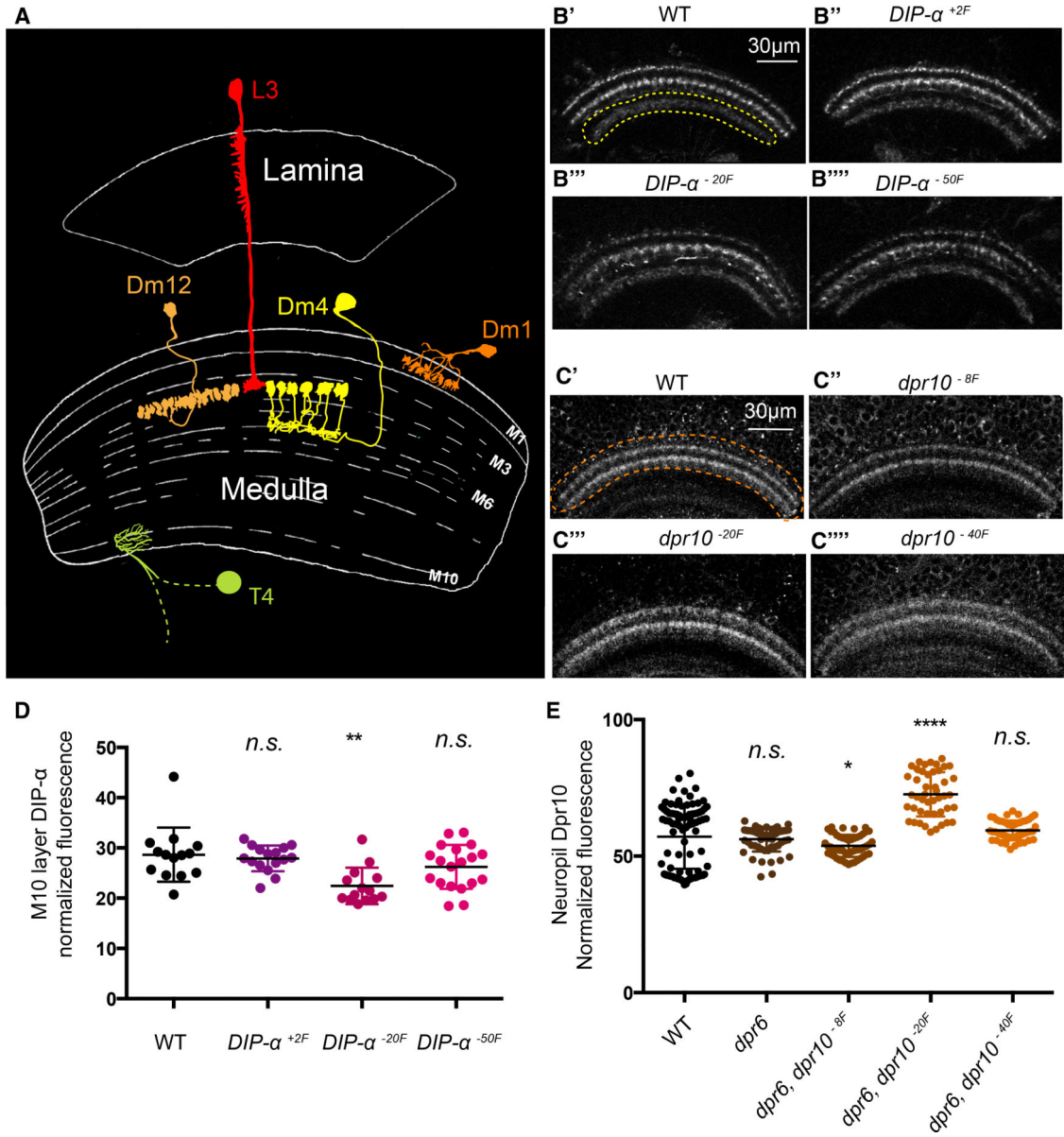


**Figure 2. DIP- $\alpha$  and Dpr10 mutant proteins are expressed in wild-type patterns and at comparable levels**

(A) Schematic of the lamina and medulla neuropil areas of adult *Drosophila* OL. The cell types studied in this paper are indicated.

(B) Anti-DIP- $\alpha$  antibody staining of medulla region in wild-type and *DIP- $\alpha$*  affinity mutants at 48 h APF. Genotypes in (B), (B''), (B'''), and (B'''): wild-type, *DIP- $\alpha$ <sup>+2F</sup>*, *DIP- $\alpha$ <sup>-20F</sup>*, and *DIP- $\alpha$ <sup>-50F</sup>*. Scale bar: 30  $\mu$ m.

(C) Anti-Dpr10 antibody staining of medulla region in wild-type and *dpr10* affinity mutants at 48 h APF. Genotypes in (C), (C'), (C''), and (C'''): wild-type, *dpr10<sup>-8F</sup>*, *dpr10<sup>-20F</sup>*, and *dpr10<sup>-40F</sup>*. Scale bar: 30  $\mu$ m.

(D) Quantification of anti-DIP- $\alpha$  fluorescence signal intensity of the most proximal medulla layer (M10) at 48 h APF (yellow dotted circle in B') in wild-type and *DIP- $\alpha$*  affinity

mutants (WT: n = 14; *DIP-α<sup>+2F</sup>*: n = 17; *DIP-α<sup>-20F</sup>*: n = 14; *DIP-α<sup>-50F</sup>*: n = 19; p value calculated against wild type; \*\*p = 0.0014; unpaired t test).

(E) Quantification of anti-Dpr10 fluorescence signal intensity of the two Dpr10-expressing neuropil layers (orange dotted circle in C') in wild-type and *dpr10* affinity mutants.

Samples were mounted dorsal up. One OL is imaged for each sample. For each sample, 15 slices of confocal images were taken starting from 50 μm away from the surface, at 5 μm step sizes. Each slice was analyzed separately for fluorescence intensity in ROI. Fluorescence intensity was normalized against background signal (number of animals quantified for each genotype: WT, n = 9; *dpr6<sup>null</sup>*, n = 6; *dpr6<sup>null</sup>*, *dpr10<sup>-8F</sup>*, n = 6; *dpr6<sup>null</sup>*, *dpr10<sup>-20F</sup>*, n = 5; *dpr6<sup>null</sup>*, *dpr10<sup>-40F</sup>*, n = 6; p value calculated against wild type; \*p = 0.0481; \*\*\*p < 0.0001; unpaired t test).

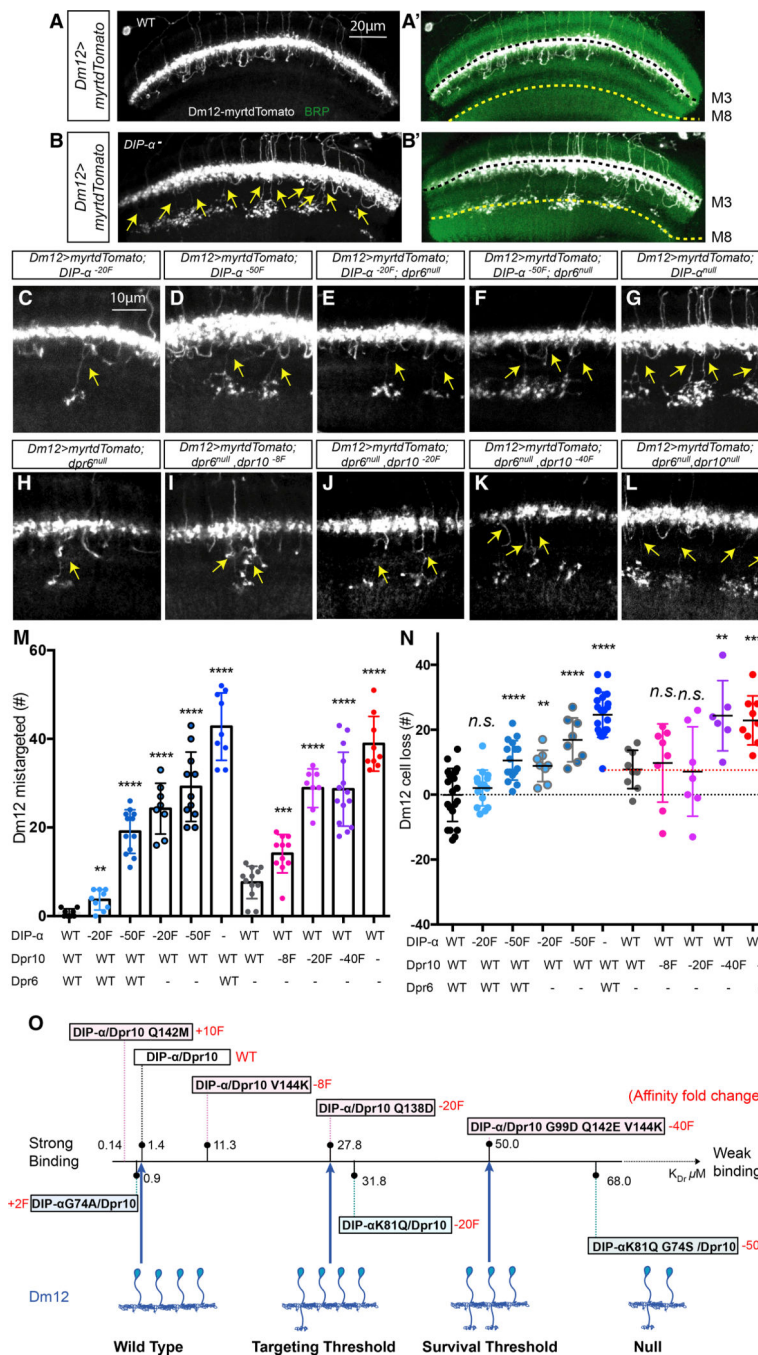


**Figure 3. *DIP-α* affinity mutants display different thresholds for Dm12 synaptic targeting and for cell survival**

(A–D) Dm12 neurons in wild-type and *DIP-α<sup>null</sup>* adult medulla. White, Dm12 neurons labeled with *Dm12-LexA > LexAop-myrtTomato*; green, anti-Bruchpilot staining showing medulla layers. Each panel is a maximum intensity projection (MIP) of a ~10 μM z stack, at 0.18 μM slice intervals, of the entire medulla neuropil. Black dotted line: M3 layer; yellow dotted line: M8 layer; yellow arrow: axons of mistargeted Dm12 neuron from M3 to M8. Scale bar: 20 μm.

(C–L) Dm12 neurons in *DIP-α* or *dpr10* affinity mutants. Genotypes as indicated. Each panel is an MIP of a ~10 μM z stack, with 0.18 μM slice intervals. Images show representative windows of the entire medulla. Yellow arrow: axons of mistargeted Dm12 neuron. Scale bar: 10 μm.

(M) Number of Dm12 neurons that mistarget to the M8 layer in wild-type and *DIP-α* mutant OLs as indicated. The number of mistargeted Dm12 neurons is quantified as the number of Dm12 axons projecting from M3 to M8 (yellow arrows, A–L; 1 OL is quantified for each animal; number of animals quantified for each genotype: WT: n = 8; *DIP-α*<sup>-20F</sup>: n = 9; *DIP-α*<sup>-50F</sup>: n = 12; *dprσ*<sup>null</sup>, *DIP-α*<sup>-20F</sup>: n = 8; *dprσ*<sup>null</sup>, *DIP-α*<sup>-50F</sup>: n = 11; *DIP-α*<sup>null</sup>: n = 9; *dprσ*<sup>null</sup>, n = 12; *dprσ*<sup>null</sup>, *dpr10*<sup>-8F</sup>: n = 11; *dprσ*<sup>null</sup>, *dpr10*<sup>-20F</sup>: n = 8; *dprσ*<sup>null</sup>, *dpr10*<sup>-40F</sup>: n = 14; *dprσ*<sup>null</sup>, *dpr10*<sup>null</sup>: n = 9; p value was calculated against wild type for flies carrying *DIP-α* mutation and against *dprσ*<sup>null</sup> for flies carrying *dprσ*<sup>null</sup> *dpr10* mutations; \*\*p < 0.01; \*\*\*p < 0.001; \*\*\*\*p < 0.0001; unpaired t test.).

(N) Number of missing Dm12 cells in wild-type and *DIP-α* affinity mutant OLs as indicated. Total number of missing Dm12 neurons was quantified as (average wild-type Dm12 neuron number) - (Dm12 neuron number in each OL). Dm12 neuron number is quantified as the number of Dm12 cell bodies in one OL (1 OL is quantified for each animal; number of animals quantified for each genotype: WT: n = 22; *DIP-α*<sup>-20F</sup>: n = 15; *DIP-α*<sup>-50F</sup>: n = 16; *dprσ*<sup>null</sup>, *DIP-α*<sup>-20F</sup>: n = 8; *dprσ*<sup>null</sup>, *DIP-α*<sup>-50F</sup>: n = 8; *DIP-α*<sup>null</sup>: n = 21; *dprσ*<sup>null</sup>, n = 9; *dprσ*<sup>null</sup>, *dpr10*<sup>-8F</sup>: n = 8; *dprσ*<sup>null</sup>, *dpr10*<sup>-20F</sup>: n = 7; *dprσ*<sup>null</sup>, *dpr10*<sup>-40F</sup>: n = 6; *dprσ*<sup>null</sup>, *dpr10*<sup>null</sup>: n = 9; p value was calculated against wild type for flies carrying *DIP-α* mutation and against *dprσ*<sup>null</sup> for flies carrying *dprσ*<sup>null</sup> *dpr10* mutations; \*\*p < 0.01; \*\*\*p < 0.001; unpaired t test).

(O) K<sub>D</sub>s of *DIP-α* and *dpr10* affinity mutant protein binding to the wild-type partner are marked on the scaled line. Dm12 targeting and cell-loss thresholds are marked at the position where a penetrance of ~50% of the null penetrance is observed.

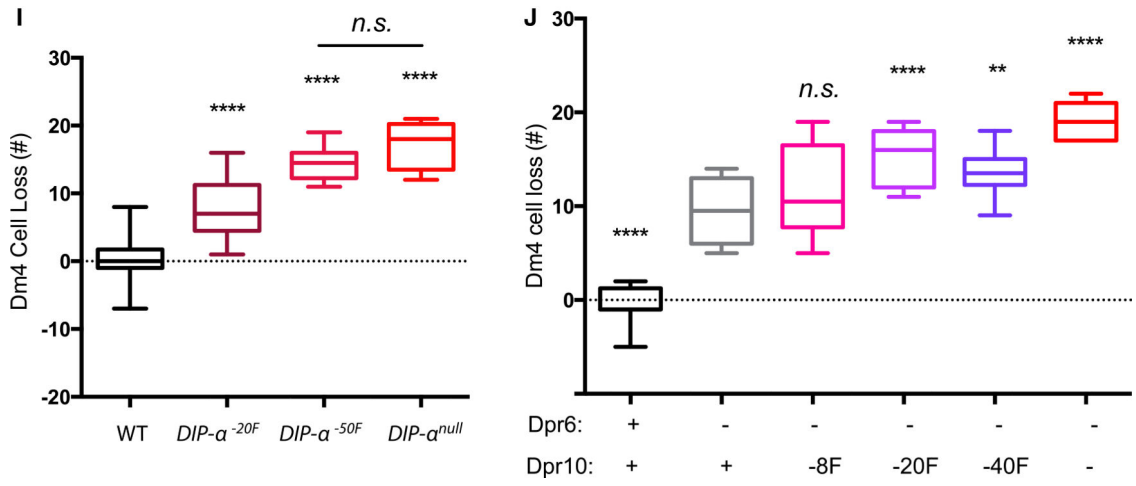
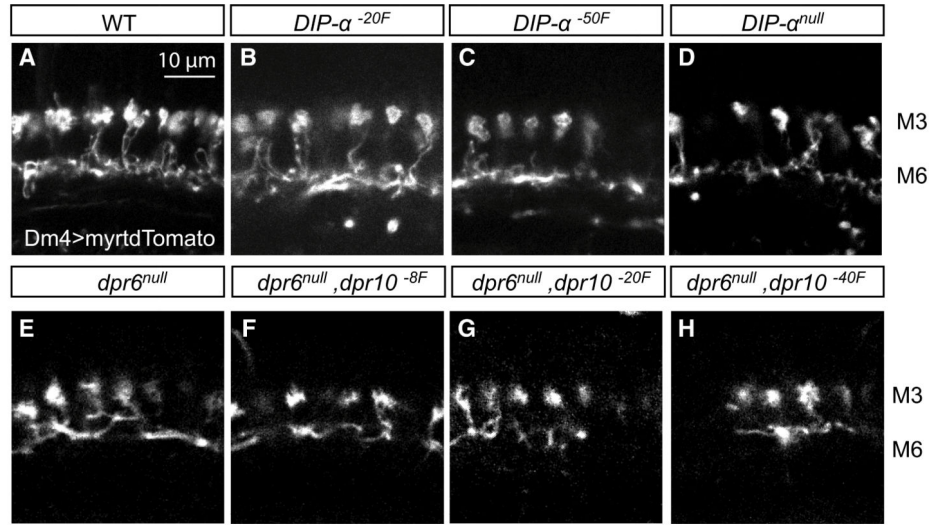


**Figure 4. Dm4 neurons show graded cell loss as DIP-α::Dpr10 affinity is reduced**  
 (A–H) Dm4 neurons are labeled by Dm4-LexA > LexAop-myrtidTomato. Each panel is a representative window of a single-slice confocal image of the medulla. Genotypes as indicated. Scale bar: 10 μm.

(I) Number of Dm4 cells lost in *DIP-α* mutants (1 OL is quantified for each animal; number of animals quantified for each genotype: WT: n = 16; *DIP-α<sup>-20F</sup>*: n = 10; *DIP-α<sup>-50F</sup>*: n = 12; *DIP-α<sup>null</sup>*: n = 6; p value calculated against wild type; \*\*\*\*p < 0.0001; unpaired t test).  
 (J) Numbers of Dm4 cells lost in *dpr6 dpr10* mutants (1 OL is quantified for each animal; number of animals quantified for each genotype: WT: n = 14; *dpr6<sup>null</sup>*, n = 10; *dpr6<sup>null</sup>, dpr10<sup>-8F</sup>*: n = 14; *dpr6<sup>null</sup>, dpr10<sup>-20F</sup>*: n = 15; *dpr6<sup>null</sup>, dpr10<sup>-40F</sup>*: n = 8; *dpr6<sup>null</sup>, dpr10<sup>null</sup>*: n = 11; p value calculated against *dpr6<sup>null</sup>*; \*\*p < 0.01; \*\*\*\*p < 0.0001; unpaired t test).

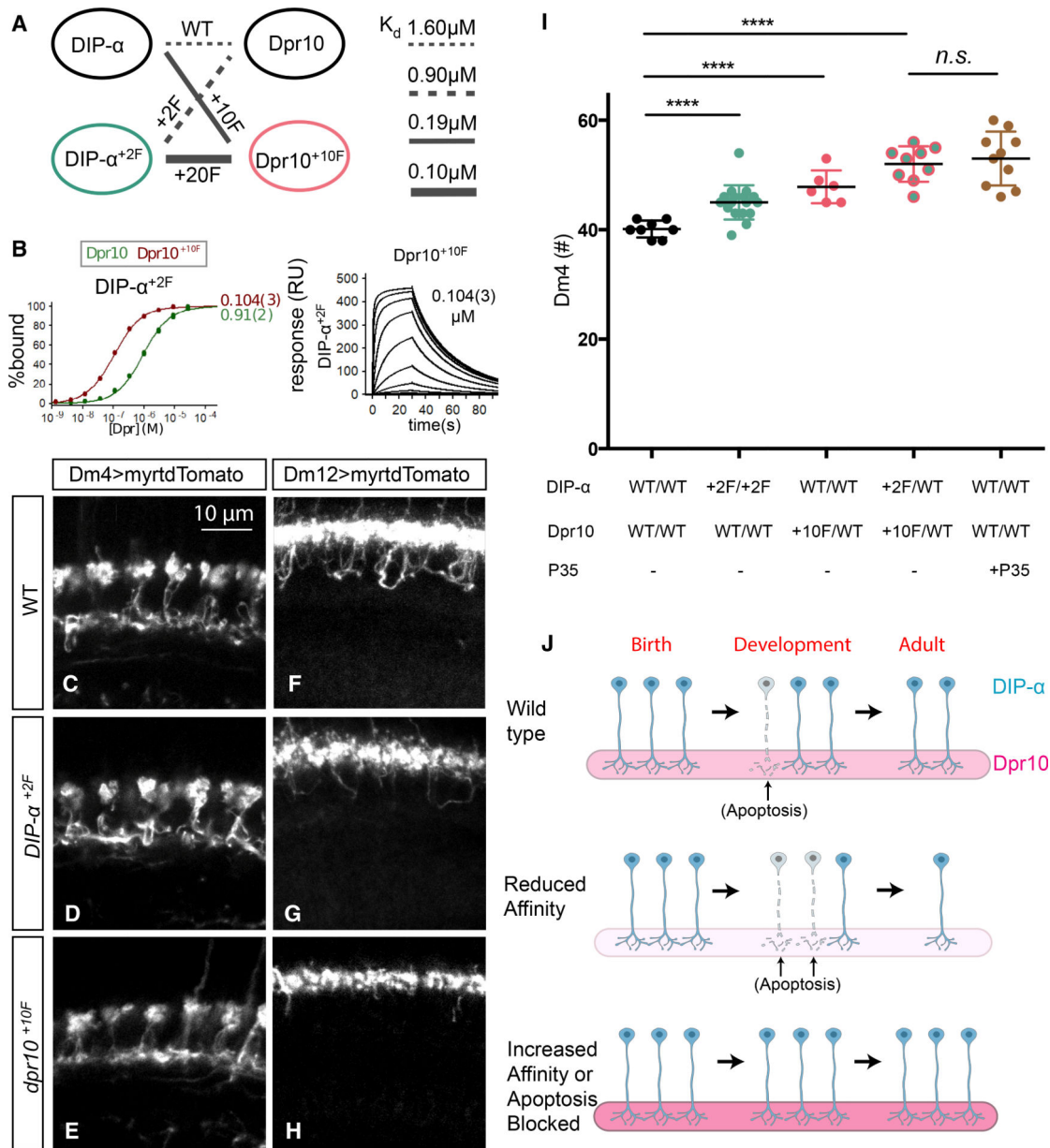


**Figure 5. Increasing DIP- $\alpha$ ::Dpr10 affinity prevents the normal culling of Dm4 neurons**  
 (A) Diagram of binding affinities among wild type and increased affinity DIP- $\alpha$  and Dpr10 mutant proteins (DIP- $\alpha^{+2F}$  and Dpr10 $^{+10F}$ ).  
 (B) Left: Dpr10 and Dpr10 $^{+10F}$  binding to DIP- $\alpha^{+2F}$ . The binding isotherms and the  $K_D$ s are color coded according to the legend shown to the bottom of the panel. Right: the binding responses between Dpr10 $^{+10F}$  and DIP- $\alpha^{+2F}$  corresponding to the SPR experiments on the left.  
 (C–H) Dm4 (C–E) or Dm12 (F–H) neurons in flies expressing wild-type or affinity-increased DIP- $\alpha$  or Dpr10 proteins. Genotypes as indicated. Dm4 neurons are labeled with Dm4-LexA > LexAop-myrtdTomato. Dm12 neurons are labeled with Dm12-LexA > LexAop-myrtdTomato. Each panel is a representative window of a single-slice confocal image of the medulla. Scale bar: 10  $\mu$ m.

(I) Numbers of Dm4 neurons in wild-type, affinity-increased, or apoptosis-blocked flies. Genotypes as indicated (1 OL is quantified for each animal; number of animals quantified for each genotype: WT: n = 8; *DIP-α<sup>+2F</sup>/DIP-α<sup>+2F</sup>*: n = 17; *dpr10<sup>+10F</sup>/WT*: n = 6; *DIP-α<sup>+2F</sup>/WT*, *dpr10<sup>+10F</sup>/WT*: n = 9; WT, +p35: n = 10; p value calculated against wild type; \*\*\*\*p < 0.0001; unpaired t test).

(J) Schematic representation of Dm4 development in wild-type, affinity-reduced mutant, affinity-increased mutant, or apoptosis-blocked flies. Saturation of the pink bar represents affinity between DIP-α and Dpr10. Gray cells represent apoptotic cells.

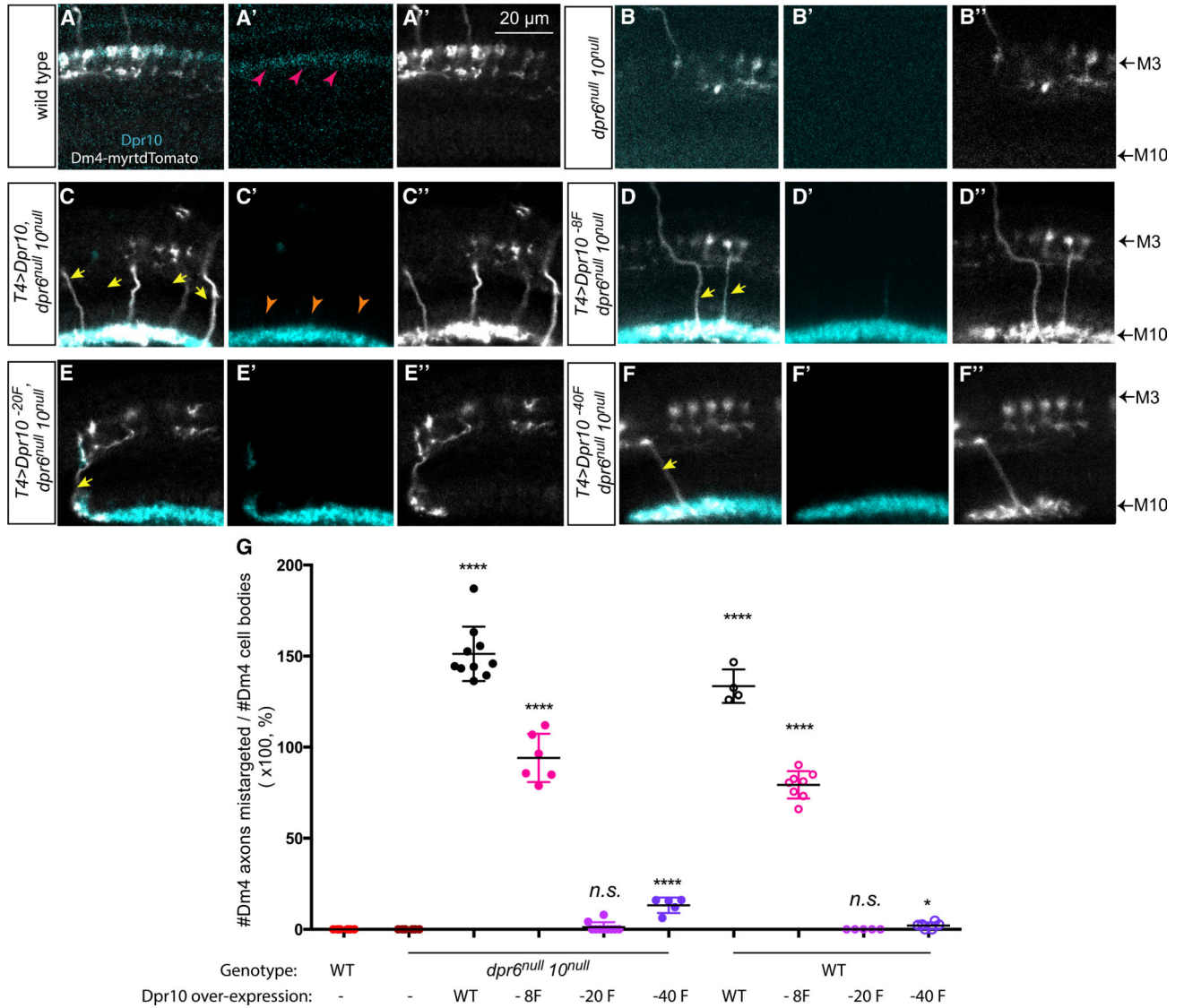


**Figure 6. An affinity threshold for induction of mistargeting by ectopic Dpr10**  
 (A–F) Dm4 neurons at 48 h APF. (A) Wild type, (B) *dpr6<sup>null</sup> dpr10<sup>null</sup>*, and (C–F) misexpression of wild-type or mutant Dpr10 proteins in M10 layer by T4-Gal4 in *dpr6<sup>null</sup>*, *dpr10<sup>null</sup>* OLs. Misexpressed proteins are as indicated. The images show one representative area of a single confocal slice of the medulla. White, Dm4 (labeled with Dm4-LexA > LexAop-myrtDTomato); cyan: Dpr10. Scale bar: 20  $\mu$ m.  
 (G) Graph summarizing (A)–(F) plus data showing overexpression of Dpr10 wild-type or mutant proteins in the wild-type background. In both genetic backgrounds, Dpr10<sup>-8F</sup> induces mistargeting, but Dpr10<sup>-20F</sup> and Dpr10<sup>-40F</sup> do not (1 OL is quantified for each animal; number of animals quantified for each genotype: WT: n = 6; *dpr6<sup>null</sup> dpr10<sup>null</sup>*: n = 6; UAS-dpr10, *dpr6<sup>null</sup> dpr10<sup>null</sup>*: n = 10; UAS-dpr10<sup>-8F</sup>, *dpr6<sup>null</sup> dpr10<sup>null</sup>*: n = 6; UAS-dpr10<sup>-20F</sup>, *dpr6<sup>null</sup> dpr10<sup>null</sup>*: n = 10; UAS-dpr10<sup>-40F</sup>, *dpr6<sup>null</sup> dpr10<sup>null</sup>*: n = 5. UAS-dpr10, *dpr6<sup>null</sup>/WT, dpr10<sup>null</sup>/WT*: n = 4; UAS-dpr10<sup>-8F</sup>, *dpr6<sup>null</sup>/WT, dpr10<sup>null</sup>/WT*: n = 8; UAS-dpr10<sup>-20F</sup>, *dpr6<sup>null</sup>/WT, dpr10<sup>null</sup>/WT*: n = 5; UAS-dpr10<sup>-40F</sup>, *dpr6<sup>null</sup>/WT*,

*dpr10<sup>null</sup>/WT*: n = 6; p value calculated against wild type; \*p = 0.0188; \*\*\*\*p < 0.0001; unpaired t test).

Author Manuscript

Author Manuscript

Author Manuscript

Author Manuscript

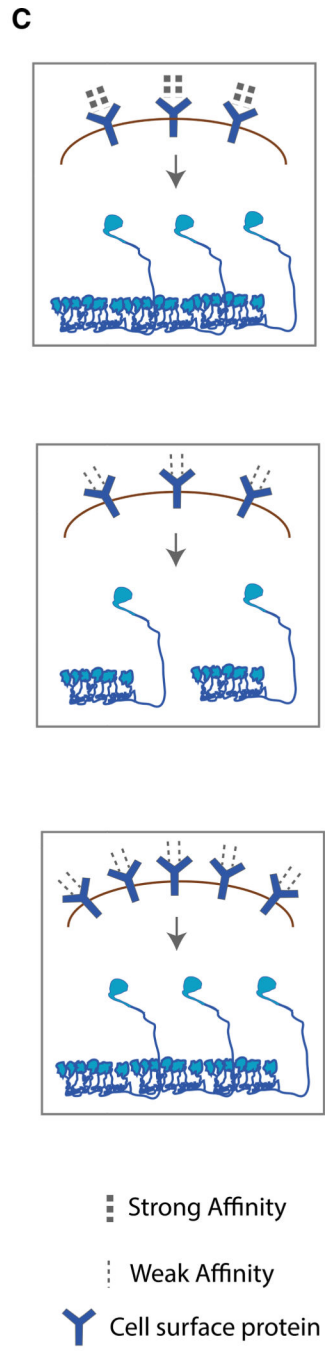
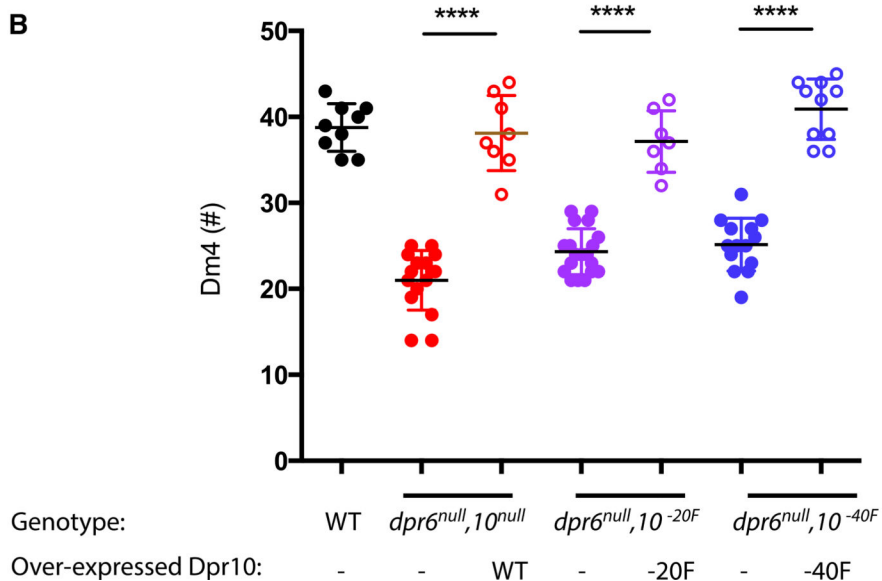
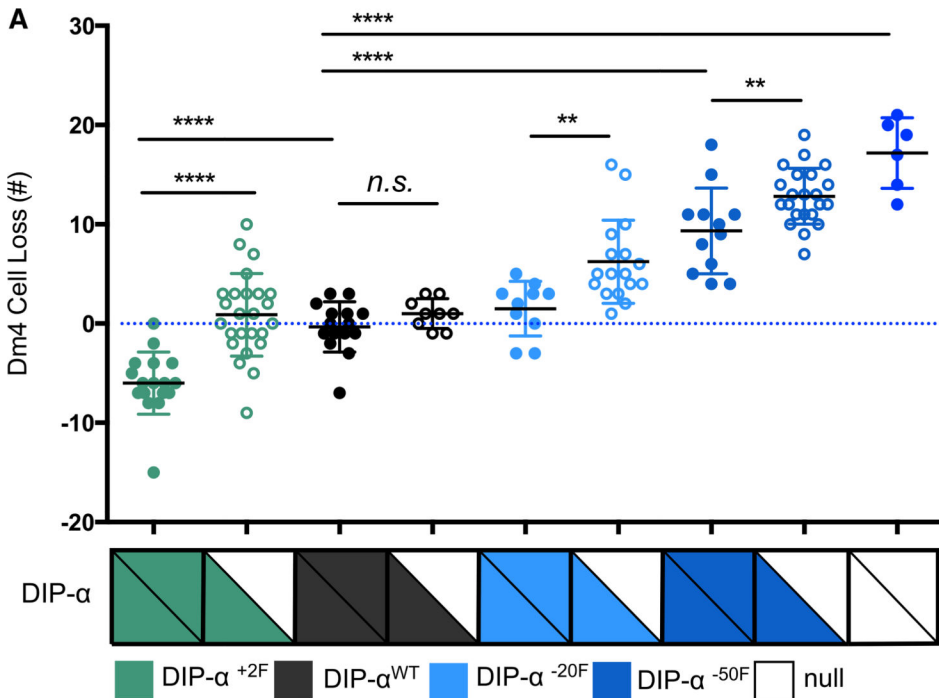


**Figure 7. Cell-surface avidity is a key parameter controlling circuit assembly**  
 (A) Numbers of Dm4 cells lost in flies expressing one or two copies of wild-type or mutant DIP- $\alpha$  proteins. Genotypes are as indicated. 1 OL is quantified for each animal. Number of animals quantified for each genotype: *DIP- $\alpha$ <sup>+2F</sup>/DIP- $\alpha$ <sup>+2F</sup>*; n = 17; *DIP- $\alpha$ <sup>+2F</sup>/WT*; n = 25; *WT*; n = 15; *WT/DIP- $\alpha$ <sup>null</sup>*; n = 9; *DIP- $\alpha$ <sup>-20F</sup>/DIP- $\alpha$ <sup>-20F</sup>*; n = 10; *DIP- $\alpha$ <sup>-20F</sup>/DIP- $\alpha$ <sup>null</sup>*; n = 16; *DIP- $\alpha$ <sup>-50F</sup>/DIP- $\alpha$ <sup>-50F</sup>*; n = 12; *DIP- $\alpha$ <sup>-50F</sup>/DIP- $\alpha$ <sup>null</sup>*; n = 22; *DIP- $\alpha$ <sup>null</sup>/DIP- $\alpha$ <sup>null</sup>*; n = 6. \*\*p = 0.0039 (*DIP- $\alpha$ <sup>-20F</sup>* group), \*\*p = 0.0075 (*DIP- $\alpha$ <sup>-50F</sup>* group), \*\*\*\*p < 0.0001, unpaired t test.

Author Manuscript

Author Manuscript

Author Manuscript

Author Manuscript

(B) Numbers of Dm4 neurons in animals overexpressing Dpr10<sup>-20F</sup> or Dpr10<sup>-40F</sup> in L3 in the indicated backgrounds (1 OL is quantified for each animal; number of animals quantified for each genotype: WT: n = 9; *dpr $\sigma$  null*, *dpr10 null*: n = 16; UAS-dpr10, *dpr $\sigma$  null*, *dpr10 null*: n = 8; *dpr $\sigma$  null*, *dpr10<sup>-20F</sup>*: n = 19; UAS-dpr10<sup>-20F</sup>, *dpr $\sigma$  null*, *dpr10<sup>-20F</sup>*: n = 7; *dpr $\sigma$  null*, *dpr10<sup>-40F</sup>*: n = 14; UAS-dpr10<sup>-40F</sup>, *dpr $\sigma$  null*, *dpr10<sup>-40F</sup>*: n = 10; \*\*\*\*p < 0.0001; unpaired t test).

(C) Schematic diagram of the effects of individual protein-protein binding affinity and protein copy number on cell survival. When cells express a reduced-affinity cell-surface protein, increased cell death is observed. Reduced affinity can be compensated by expressing more copies of the same protein.

## KEY RESOURCES TABLE

REAGENT or RESOURCE	SOURCE	IDENTIFIER
Antibodies		
chicken-anti-GFP	Abcam	Cat#ab13970; RRID:AB_300798
rabbit-anti-DsRed	Clontech	Cat#632496; RRID:AB_10013483
chicken-anti-V5	Abcam	Cat#9113; RRID:AB_307022
mouse-anti-DIP- $\alpha$	Xu. et al., 2018	N/A
mouse-anti-Dpr10	Xu. et al., 2018	N/A
Alexa Fluor 488 donkey-anti-chicken	Jackson Immuno Research Lab	Cat#703-545-155; RRID:AB_2340375
Alexa Fluor 488 donkey-anti-mouse	Jackson Immuno Research Lab	Cat#715-545-151; RRID:AB_2341099
Alexa Fluor 594 donkey-anti-rabbit	Jackson Immuno Research Lab	Cat#711-585-152; RRID:AB_2340621
Alexa Fluor 647 donkey-anti-rat	Jackson Immuno Research Lab	Cat#712-605-153; RRID:AB_2340694
Alexa Fluor 647 donkey-anti-mouse	Jackson Immuno Research Lab	Cat#715-605-151; RRID:AB_2340863
Bacterial and virus strains		
One shot Top10 Competent Cells	Invitrogen	C4040-06
Chemicals, peptides, and recombinant proteins		
All Dpr and DIP proteins	Sergeeva et al. (2020), this paper	N/A
Everbrite Mounting Reagent	Biotium	Cat#23001
Para-formaldehyde	Electron Microscopy Sciences	Cat#15713-s
LE Agarose	Apex	Cat#20-102GP
Ethidium Bromide	VWR	Cat#1239-45-8
Tris Base	Fisher Scientific	Cat# BP152-5
Sodium Chloride	Fisher Scientific	Cat# S271-10
Calcium Chloride Dihydrate	JT Baker	Cat# 1336-01
EDTA	ACROS	Cat# 409930010
BIS-Tris	Sigma	Cat# B9754
HEPES	Sigma	Cat# H3375
Imidazole	ACROS	Cat# 301870025
BSA	Sigma	Cat# A7906
Polyethylenimine	Polysciences	Cat# 24765-2
N-Hydroxysuccinimide	Thermo Fisher Scientific	Cat# 24500
1-Ethyl-3-(3-dimethylaminopropyl) carbodiimide	Thermo Fisher Scientific	Cat# 22980
Sodium Acetate	Sigma	Cat# S7545
Ethanolamine	Sigma	Cat# 398136
Tween-20	Sigma	Cat# P7949
Freestyle™ 293 Expression Media	Thermo Fisher Scientific	Cat# 12338-018
Opti-MEM™ Reduced Serum Media	Thermo Fisher Scientific	Cat# 31985-070
Fetal Bovine Serum, qualified, heat inactivated, US origin	Thermo Fisher Scientific	Cat# 16140071
IMAC Sepharose 6 Fast Flow	Cytiva	Cat# 17092109

REAGENT or RESOURCE	SOURCE	IDENTIFIER
Series S CM4 chip	Cytiva	Cat# BR100539
Critical commercial assays		
2x Gibson Assembly Master Mix	New England Biolabs	Cat#E2611L
Dreamtaq Green PCR Master Mix	Thermo Scientific	Cat#K1081
NotI restriction enzyme	New England Biolabs	Cat#R0189S
XbaI restriction enzyme	New England Biolabs	Cat#R0145S
Spin Miniprep Kit	Qiagen	Cat# 27106
HiSpeed Plasmid Maxi Kit	Qiagen	Cat# 12663
Experimental Models: Cell Lines		
Human: FreeStyle™ 293-F cells	Thermo Fisher Scientific	Cat# R79007
Experimental models: Organisms/strains		
<i>D. melanogaster</i> : 24F10-GAL4	Bloomington Drosophila Stock Center	BDSC: 49090; RRID:BDSC_49090
<i>D. melanogaster</i> : 75F06-GAL4	Bloomington Drosophila Stock Center	BDSC: 39901; RRID:BDSC_39901
<i>D. melanogaster</i> : 23G11-LexA	Bloomington Drosophila Stock Center	BDSC: 54775; RRID:BDSC_54775
<i>D. melanogaster</i> : 24F10-LexA	Bloomington Drosophila Stock Center	BDSC: 52696; RRID:BDSC_52696
<i>D. melanogaster</i> : 75F06-LexA	Bloomington Drosophila Stock Center	BDSC: 54100; RRID:BDSC_54100
<i>D. melanogaster</i> : 47G08-GAL4	Bloomington Drosophila Stock Center	BDSC: 50328; RRID:BDSC_50328
<i>D. melanogaster</i> : 9B08-GAL4	Bloomington Drosophila Stock Center	BDSC: 41369; RRID:BDSC_41369
<i>D. melanogaster</i> : 42F06-GAL4	Bloomington Drosophila Stock Center	BDSC: 41253; RRID:BDSC_41253
<i>D. melanogaster</i> : 9D03-GAL4	Bloomington Drosophila Stock Center	BDSC: 47364; RRID:BDSC_47364
<i>D. melanogaster</i> : 13xLexAop-CD4-tdTom (attp2)	Xu. et al. (2018)	N/A
<i>D. melanogaster</i> : 10xUAS-myr::GFP (attP2; attP40)	Xu. et al. (2018)	N/A
<i>D. melanogaster</i> : LexAop-myr::GFP	Xu. et al. (2018)	N/A
<i>D. melanogaster</i> : LexAopmyrtdTomato	Xu. et al. (2018)	N/A
<i>D. melanogaster</i> : UAS-P35	Pecot et al. (2014)	This lab
<i>D. melanogaster</i> : <i>DIP-α<sup>null1</sup></i>	Xu. et al. (2018)	N/A
<i>D. melanogaster</i> : <i>dpr6<sup>null</sup></i>	Xu. et al. (2018)	N/A
<i>D. melanogaster</i> : <i>dpr10<sup>null</sup></i>	Xu. et al. (2018)	N/A
<i>D. melanogaster</i> : <i>dpr6-10<sup>L</sup></i>	Xu. et al. (2018)	N/A
<i>D. melanogaster</i> : UAS-Dpr10D.NV5	Xu. et al. (2018)	N/A
<i>D. melanogaster</i> : <i>DIP-α<sup>+2F</sup></i>	This paper	N/A
<i>D. melanogaster</i> : <i>DIP-α<sup>-20F</sup></i>	This paper	N/A
<i>D. melanogaster</i> : <i>DIP-α<sup>-50F</sup></i>	This paper	N/A

REAGENT or RESOURCE	SOURCE	IDENTIFIER
<i>D. melanogaster</i> : <i>dpr10<sup>-10F</sup></i>	This paper	N/A
<i>D. melanogaster</i> : <i>dpr10<sup>-8F</sup></i>	This paper	N/A
<i>D. melanogaster</i> : <i>dpr10<sup>-20F</sup></i>	This paper	N/A
<i>D. melanogaster</i> : <i>dpr10<sup>-40F</sup></i>	This paper	N/A
<i>D. melanogaster</i> : UAS-Dpr10D <sup>-8F</sup> .NV5	This paper	N/A
<i>D. melanogaster</i> : UAS-Dpr10D <sup>-20F</sup> .NV5	This paper	N/A
<i>D. melanogaster</i> : UAS-Dpr10D <sup>-40F</sup> .NV5	This paper	N/A
Oligonucleotides		
Primers used for making affinity mutations are listed in Table S3.	This paper	N/A
Recombinant DNA		
VRC-8400	Vaccine Research Center (NIH), Gary Nabel	N/A
Software and algorithms		
Imaris 8.2.0	Bitplane	<a href="http://www.bitplane.com/imaris">http://www.bitplane.com/imaris</a>
Fiji	Schindelin et al. (2012)	<a href="http://fiji.sc/">http://fiji.sc/</a>
Prism	Graphpad	<a href="https://www.graphpad.com/scientific-software/prism/">https://www.graphpad.com/scientific-software/prism/</a>
Scrubber 2.0	BioLogic Software	<a href="http://www.biologic.com.au">http://www.biologic.com.au</a>